iScience

CellPress
OPEN ACCESS

Article

Exome Sequencing Implicates Impaired GABA Signaling and Neuronal Ion Transport in Trigeminal Neuralgia

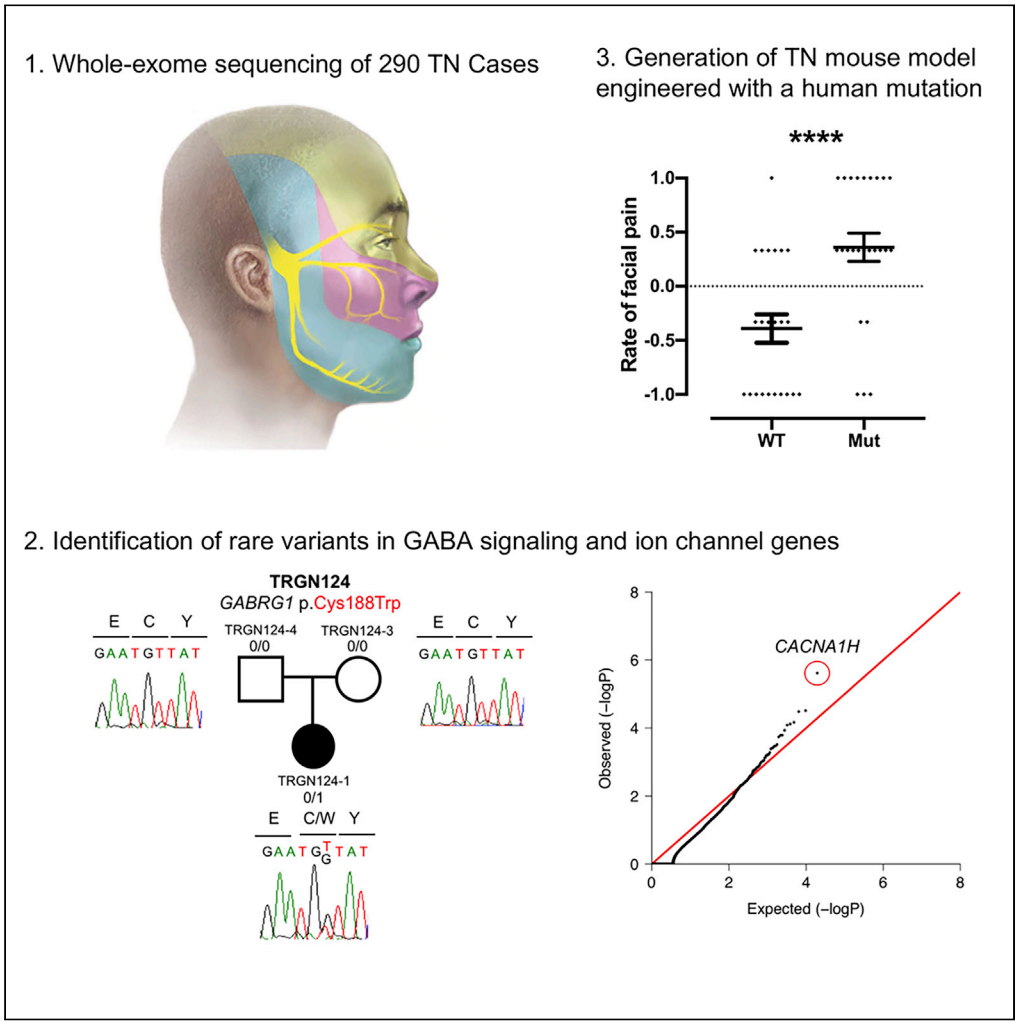

Weilai Dong, Sheng Chih Jin, August Allocco, ..., Yves De Koninck, Richard P. Lifton, Kristopher T. Kahle

kristopher.kahle@yale.edu

HIGHLIGHTS

Genomic analysis of trigeminal neuralgia (TN) using exome sequencing

Rare mutations in GABA signaling and ion transport genes are enriched in TN cases

Generation of a genetic TN mouse model engineered with a patient-specific mutation

Dong et al., iScience 23, 101552
October 23, 2020
https://doi.org/10.1016/j.isci.2020.101552

iScience

CellPress
OPEN ACCESS

Article

Exome Sequencing Implicates Impaired GABA Signaling and Neuronal Ion Transport in Trigeminal Neuralgia

Weilai Dong,[1,2,27] Sheng Chih Jin,[3,27] August Allocco,[4,27] Xue Zeng,[1,2,27] Amar H. Sheth,[4] Shreyas Panchagnula,[4] Annie Castonguay,[5] Louis-Étienne Lorenzo,[5] Barira Islam,[6] Geneviève Brindle,[5] Karine Bachand,[5] Jamie Hu,[4] Agata Sularz,[4] Jonathan Gaillard,[4] Jungmin Choi,[1,2,7] Ashley Dunbar,[4] Carol Nelson-Williams,[1] Emre Kiziltug,[4] Charuta Gavankar Furey,[4] Sierra Conine,[4] Phan Q. Duy,[4] Adam J. Kundishora,[4] Erin Loring,[1] Boyang Li,[8] Qiongshi Lu,[9] Geyu Zhou,[26] Wei Liu,[26] Xinyue Li,[25] Michael C. Sierant,[1,2] Shrikant Mane,[10] Christopher Castaldi,[10] Francesc López-Giráldez,[10] James R. Knight,[10] Raymond F. Sekula, Jr.,[11] J. Marc Simard,[12] Emad N. Eskandar,[13] Christopher Gottschalk,[14] Jennifer Moliterno,[4] Murat Günel,[4] Jason L. Gerrard,[4] Sulayman Dib-Hajj,[15,16] Stephen G. Waxman,[15,16] Fred G. Barker II,[17,18,19] Seth L. Alper,[20] Mohamed Chahine,[5,21] Shozeb Haider,[6] Yves De Koninck,[5,22] Richard P. Lifton,[1,2] and Kristopher T. Kahle[4,23,24,28,29,*]

SUMMARY

Trigeminal neuralgia (TN) is a common, debilitating neuropathic face pain syndrome often resistant to therapy. The familial clustering of TN cases suggests that genetic factors play a role in disease pathogenesis. However, no unbiased, large-scale genomic study of TN has been performed to date. Analysis of 290 whole exome-sequenced TN probands, including 20 multiplex kindreds and 70 parent-offspring trios, revealed enrichment of rare, damaging variants in GABA receptor-binding genes in cases. Mice engineered with a TN-associated *de novo* mutation (p.Cys188Trp) in the $GABA_A$ receptor Cl^- channel γ-1 subunit (*GABRG1*) exhibited trigeminal mechanical allodynia and face pain behavior. Other TN probands harbored rare damaging variants in Na^+ and Ca^+ channels, including a significant variant burden in the α-1H subunit of the voltage-gated Ca^{2+} channel $Ca_v3.2$ (*CACNA1H*). These results provide exome-level insight into TN and implicate genetically encoded impairment of GABA signaling and neuronal ion transport in TN pathogenesis.

INTRODUCTION

Trigeminal neuralgia (TN), or "tic doulourex," is a severe neuropathic face pain syndrome characterized by recurrent, paroxysmal, lancinating face pain in the distribution of the trigeminal nerve that is variably triggered by sensory stimuli such as light touch or cold temperature (Maarbjerg et al., 2017). TN affects ~3–4 per 100,000 people in the United States (Katusic et al., 1991; MacDonald et al., 2000). The pathogenesis of "classical TN (cTN)" is frequently attributed to hyperexcitability of trigeminal ganglion neurons (Burchiel, 1980a, 1980b; Burchiel and Baumann, 2004; Devor et al., 2002) secondary to morphological compression of the trigeminal nerve root entry root by the cerebral vasculature (i.e., neurovascular compression [NVC]) (Headache Classification Committee of the International Headache Society (IHS), 2013; Cruccu et al., 2016; Gardner and Miklos, 1959; Hilton et al., 1994; Rappaport et al., 1997). However, asymptomatic NVC has been noted in ~13%–85% of asymptomatic subjects (Haines et al., 1980; Hamlyn, 1997a, 1997b; Jani et al., 2019). Other cases of TN are related to trigeminal nerve infection (e.g., herpes zoster), trauma, demyelination (as in multiple sclerosis), or compression from a space-occupying lesion in the cerebellopontine angle and are termed "secondary TN." However, a significant number of TN cases lack a demonstrable cause ("idiopathic TN [iTN]") (Hughes et al., 2019; Maarbjerg et al., 2017), including some cases with bilateral symptoms (Brisman, 1987; Pollack et al., 1988).

First-line pharmacotherapy of TN includes the Na^+ channel blocker carbamazepine or its analogs (Al-Quliti, 2015), followed by other Na^+ channel- or GABA-modulating anticonvulsants such as gabapentin,

Continued

[1]Department of Genetics, Yale School of Medicine, New Haven, CT, USA

[2]Laboratory of Human Genetics and Genomics, The Rockefeller University, New York, NY, USA

[3]Department of Genetics, Washington University School of Medicine, St. Louis, MO, USA

[4]Department of Neurosurgery, Yale School of Medicine, New Haven, CT, USA

[5]CERVO Brain Research Centre, Université Laval, Québec, QC, Canada

[6]University College London, School of Pharmacy, London, England

[7]Department of Biomedical Sciences, Korea University College of Medicine, 02841 Seoul, Korea

[8]Department of Biostatistics, Yale School of Public Health, New Haven, CT, USA

[9]Department of Biostatistics & Medical Informatics, University of Wisconsin-Madison, Madison, WI, USA

[10]Yale Center for Genome Analysis, West Haven, CT, USA

[11]Department of Neurological Surgery, University of Pittsburgh School of Medicine and University of Pittsburgh Medical Center, Pittsburgh, PA, USA

lamotrigine, and topiramate (Ahmed et al., 2012). The efficacy of these drugs suggests that neuronal hyperexcitability and aberrant ion transport may be involved in TN pathogenesis. For patients resistant to medical therapy, alternative interventional and surgical treatments are offered. These include neurolysis of the trigeminal ganglion and the cisternal segment of the nerve, as well as open neurosurgical microvascular decompression (MVD) of the nerve. However, the few reported randomized, placebo-controlled trials with long-term follow-up have left continued uncertainty about the efficacy of these medical and surgical interventions (Zakrzewska and Akram, 2011). Gaps in our understanding of the cellular and molecular pathogenesis of TN have impeded the development of improved diagnostic, prognostic, and therapeutic measures.

The reported heritability of neuropathic pain conditions ranges from 16% to 50% (Hocking et al., 2012; Nielsen et al., 2012). Familial forms of TN are well documented, with many exhibiting autosomal dominant inheritance with incomplete penetrance (El Otmani et al., 2008; Rodriguez et al., 2019; Fleetwood et al., 2001; Smyth et al., 2003). The average age of onset in familial forms is 44.4 years (Fleetwood et al., 2001), 9 years younger than the average age of sporadic TN cases (Maarbjerg et al., 2015). A subset of familial forms demonstrates genetic anticipation, with progressively earlier disease onset across each succeeding generation (Harris, 1936; Smyth et al., 2003). These observations implicate genetic determinants in TN pathogenesis. Previous studies using candidate gene approaches have identified an association of TN with a common SNP in the Na^+-dependent serotonin transporter SERT (*SLC6A4*) (Cui et al., 2014) and a gain-of-function *de novo* mutation (DNM) in the voltage-gated Na^+ channel Nav1.6 (*SCN8A*) in a single patient with TN (Tanaka et al., 2016). However, no large, unbiased, whole-exome sequencing (WES) genomics study of TN has been performed to date.

The discovery of human genetic variants associated with TN could illuminate disease mechanisms, explain the variability of TN phenotypes and therapeutic responses, and identify potential drug targets for therapeutic intervention. Here, we present our analysis of WES of 290 TN probands, including 20 multiplex kindreds and 70 parent-offspring trios. This approach, proven to be successful for several neurodevelopmental disorders (Allen et al., 2013; Furey et al., 2018; Iossifov et al., 2012; Vissers et al., 2010), congenital heart disease (Jin et al., 2017; Zaidi et al., 2013), and other heritable conditions (Duran et al., 2019; Furey et al., 2018; Timberlake et al., 2016), enables unbiased identification of rare, damaging DNMs and copy number variations (CNVs), along with rare, inherited single-nucleotide variants and insertions and deletions (indels) that contribute to disease pathogenesis. We hypothesized that rare, damaging variants in genes encoding proteins with important roles in the development, structure, or function of neurons in the peripheral or central trigeminal pain circuitry might confer risk for the development of TN.

RESULTS

Cohort Characteristics and Whole-Exome Sequencing

We ascertained 290 probands with TN-related disorders, including 41 from the UK Biobank (Table 1). UK Biobank patients included 34 singleton probands (85.4%) with a primary diagnosis of TN (ICD10 code: G50.0), 6 singleton probands (17.1%) with atypical facial pain (ICD10 code: G50.1), and one singleton proband with both. We recruited an additional 249 probands with either cTN, iTN type 1 (purely paroxysmal) or type 2 (with concomitant continuous pain) that included 70 parent-offspring trios; 63.9% (159/249) of probands had undergone neurosurgical intervention, including MVD (54.6%, 136/249), thermal or balloon rhizotomy (11.6%, 29/249), or gamma knife radiosurgery (14.9%, 37/249). Of the patients treated with MVD, 42.6% (58/136) did not have sustained symptom relief; 19.1% (26/136) of these patients underwent a repeat MVD for post-operative recurrence of symptoms. Interestingly, 36/249 (14.5%) cases were characterized by bilateral TN and 41/249 (16.5%) probands had a family history of TN.

Variants in Genes Previously Associated with TN

To gain insight into the genetic architecture of TN, we first screened for rare, damaging heterozygous mutations (minor allele frequency [MAF] $\leq 1 \times 10^{-3}$ in Bravo) (Program, 2018) in genes previously implicated in TN (Cui et al., 2014; Tanaka et al., 2016). Two probands each carried a deleterious missense (predicted as deleterious by MetaSVM or having a CADD score $\geq$ 30; D-mis) (Dong et al., 2015; Kircher et al., 2014) mutation in non-conserved residues of *SCN8A*. p.Ile1583Thr maps to the ion transport domain, and p.Arg475Gln is located immediately adjacent to the voltage-gated Na^+ channel domain (Figures S1A and S1B). No rare damaging mutations were identified in *SLC6A4*.

[12]Department of Neurosurgery, University of Maryland School of Medicine, Baltimore, MD, USA

[13]Department of Neurological Surgery, Albert Einstein College of Medicine, Montefiore Medical Center, New York

[14]Headache Medicine, Department of Neurology, Yale School of Medicine, New Haven, CT, USA

[15]Center for Neuroscience & Regeneration Research, VA Connecticut Healthcare System, West Haven, CT, USA

[16]Department of Neurology; Yale University, New Haven, CT, USA

[17]Harvard Medical School, Boston, MA, USA

[18]Cancer Center, Massachusetts General Hospital, Boston, MA, USA

[19]Department of Neurosurgery, Massachusetts General Hospital, Boston, MA, USA

[20]Division of Nephrology and Center for Vascular Biology Research, Beth Israel Deaconess Medical Center, and Department of Medicine, Harvard Medical School, Boston, MA, USA

[21]Department of Medicine, Université Laval, Québec, QC, Canada

[22]Department of Psychiatry and Neuroscience, Université Laval, Québec, QC, Canada

[23]Department of Pediatrics, Yale School of Medicine, New Haven, CT, USA

[24]Department of Cellular & Molecular Physiology, Yale School of Medicine, New Haven, CT, USA

[25]School of Data Science, City University of Hong Kong, Hong Kong, China

[26]Program of Computational Biology and Bioinformatics, Yale University, New Haven, CT, USA

[27]These authors contributed equally

[28]Senior author

[29]Lead Contact

*Correspondence: kristopher.kahle@yale.edu

https://doi.org/10.1016/j.isci.2020.101552

	TN Cases from Yale	TN Cases from UK BioBank	Autism Sibling Controls
Sample size	249	41	1,798
Trios	70 (28.1%)	0 (0.0%)	1,798 (100.0%)
Non-trio cases	179 (71.9%)	41 (100.0%)	0 (0.0%)
Cases with family history of TN	41 (16.5%)	NA	NA
Cases with ≥ 2 affected members sequenced	20 (8.0%)	NA	NA
Gender			
Male	34 (13.7%)	15 (36.6%)	842 (46.8%)
Female	215 (86.3%)	26 (63.4%)	956 (53.2%)
Ethnicity			
European	238 (95.6%)	38 (92.7%)	1,418 (78.9%)
African American	0 (0.0%)	1 (2.4%)	77 (4.3%)
East Asian	1 (0.4%)	1 (2.4%)	40 (2.2%)
South Asian	1 (0.4%)	0 (0.0%)	88 (4.9%)
Mexican	6 (2.4%)	1 (2.4%)	129 (7.2%)
Other	3 (1.2%)	0 (0.0%)	46 (2.6%)
TN type			
cTN-1	47 (18.9%)	NA	NA
cTN-2	80 (32.1%)	NA	NA
iTN-1	44 (17.7%)	NA	NA
iTN-2	78 (31.3%)	NA	NA
Bilateral symptoms	36 (14.5%)	NA	NA
Neurosurgical intervention	159 (63.9%)	NA	NA
MVD	136 (54.6%)	NA	NA
With relief of symptoms	75 (30.1%)	NA	NA
No relief of symptoms	58 (23.3%)	NA	NA
Repeated MVD	26 (10.4%)	NA	NA
Thermal or balloon rhizotomy	29 (11.6%)	NA	NA
Gamma knife	37 (14.9%)	NA	NA
Other	22 (8.8%)	NA	NA

Table 1. Demographic and clinical characteristics of TN cases and controls

The number of samples is shown in each category with the corresponding percentage in parentheses. Some Trios contain ≥ 2 affected members. Ethnicity is determined by principal component analysis compared to HapMap samples using EIGENSTRAT. See also Figure S4.

Familial Forms of TN and *SCN5A* Variants

We next examined rare (MAF $\leq 5 \times 10^{-4}$) damaging (i.e., D-mis or loss-of-function [LoF]) variants that segregated with TN in 20 multiplex families with at least two affected individuals available for WES (Figure 1). Of the 10 genes with segregating variants in at least two families (Table S1A), only *SCN5A*, encoding Na^+ channel Nav1.5, was intolerant to both LoF (pLI ≥ 0.9) and missense variants (missense z-score ≥ 2) (Figures S1C and S1D). In iTN-1 family TRGN201, *SCN5A* p.Arg1826His was shared by affected siblings

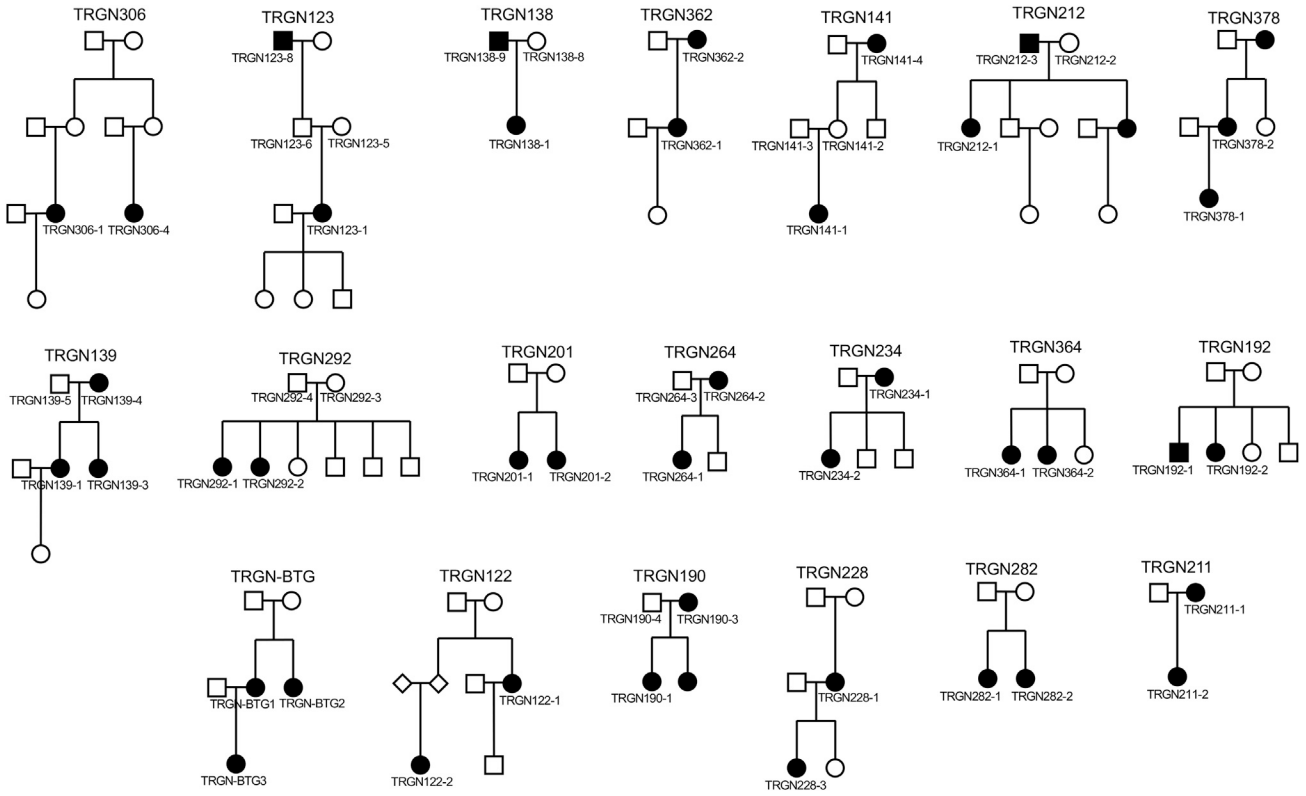

Figure 1. Pedigrees for 20 TN Familial Cases

20 familial cases with ≥2 members available for whole-exome sequencing (WES) are shown with sample IDs. Black circle/squares: Subjects with TN diagnosis. See also Table S1.

TRGN201-1 and TRGN201-2 (Figure S1E). p.Arg1826His maps to a conserved residue in the Nav1.5 C-terminal cytoplasmic domain and is reported in ClinVar as pathogenic for long QT syndrome (Figure S1D). Nav1.5 Arg1826His-mediated Na^+ currents exhibit delayed inactivation and a 2- to 3-fold increase in late Na^+ current (Ackerman et al., 2001; Wei et al., 2013). *SCN5A* p.Phe1293Ser was shared by cTN-1 proband TRGN141-1 and her affected maternal grandmother TRGN141-4 (Figure S1E). p.Phe1293Ser maps to *SCN5A* domain III and is predicted to alter Nav1.5 structure (Figure S1D). Of note, *SCN5A*-mutant TN patients did not report a history of cardiac arrhythmias or sudden death (Roberts, 2006).

Copy Number Variation in Familial TN

We also identified four rare CNVs (MAF $\leq 1 \times 10^{-3}$) that segregated in three multiplex TN families (Table S1B). Among them, one ~500-kb duplication covering the serine-threonine kinase *MAPK3* was shared by the proband and the affected mother, but not the unaffected father in family TRGN190. *MAPK3* has been previously implicated in the pathogenesis of multiple trigeminal pain models (Alter et al., 2010; Liverman et al., 2009; Smyth et al., 2003; Sun et al., 2019). Interestingly, the TRGN190 proband with the *MAPK3* duplication was diagnosed with bilateral cTN-1 at 11 years of age and exhibited bilateral NVC on brain magnetic resonance imaging (MRI). The patient was treated with bilateral MVD, followed 1 year later by repeat bilateral MVD for symptom recurrence. The proband's mother, also with an *MAPK3* duplication, was diagnosed with bilateral cTN-1 at 43 years of age. Although NVC was observed on her MRI, she declined surgery. Both patients reported significant symptom relief with the voltage-gated Na^+ channel blocker oxcarbazepine. The proband's sister was also diagnosed with oxcarbazepine-responsive unilateral iTN at 17 years of age, but was not available for WES.

Rare, Damaging *De Novo* and Inherited Variants in GABA Signaling Genes

We next examined the contribution of DNMs, including CNVs, to TN risk. Our TN cohort demonstrated a rate of 1.06 coding region DNMs per proband, following the expected Poisson distribution and closely

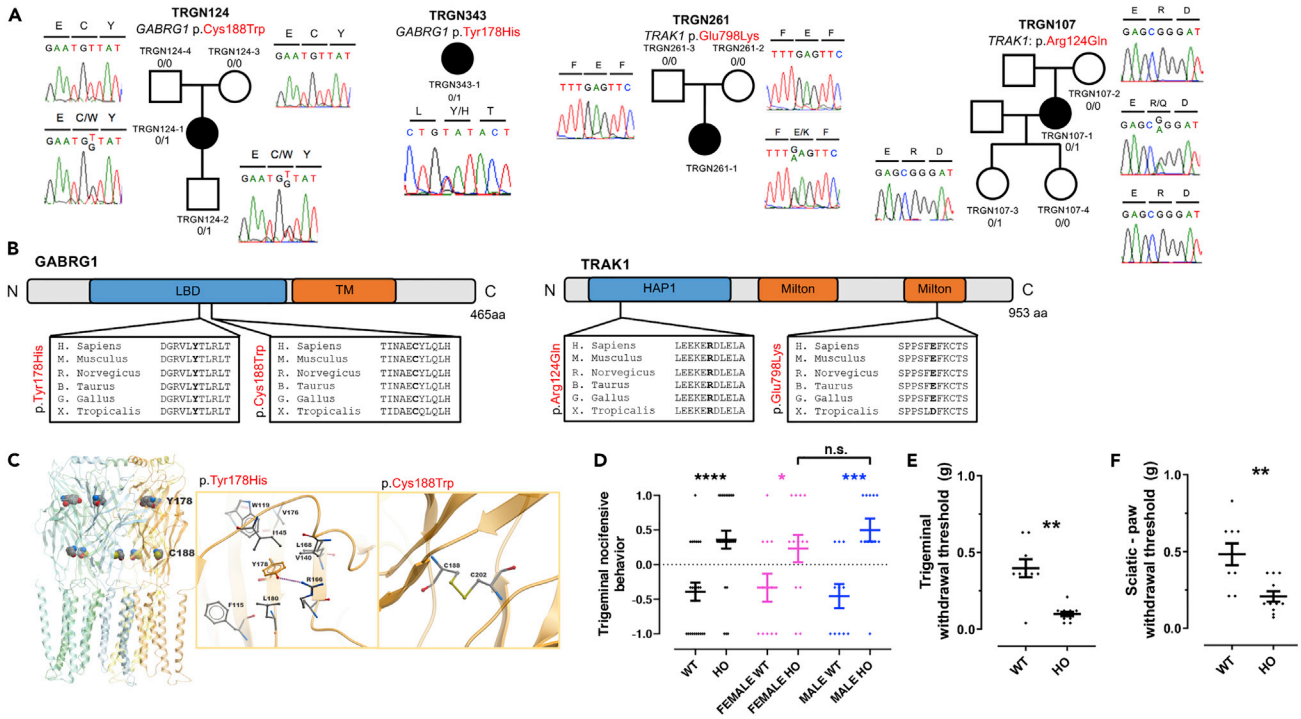

Figure 2. Damaging *De Novo* and Inherited Mutations in *GABRG1* and *TRAK1* in TN Probands

(A) *De novo* and inherited mutations in *GABRG1* and *TRAK1*. Pedigrees with Sanger-validated mutant bases marked on the chromatograms.

(B) Mapping of *GABRG1* and *TRAK1* mutations. *GABRG*1 p.Cys188Trp and p.Tyr178His impact conserved residues at the neurotransmitter-gated ligand-binding domain of *GABRG1*. *TRAK1* p.Glu798Lys affects a conserved residue of the second kinesin-binding Milton domain, whereas *TRAK1* p.Arg124Gln maps to a conserved residue of the HAP1_N domain.

(C) Structural modeling of *GABRG1* p.Cys188Trp and p.Tyr178His mutations. p.Cys188 disulfide bonds with Cys202. Mutation to Trp188 disrupts this conserved disulfide bond with calculated $\Delta\Delta G$ = 3.8 kcal/mol. In the midst of surrounding hydrophobic residues, the side chain hydroxyl of Tyr178 hydrogen bonds with the guanidinium side chain of Arg166, stabilizing interactions between their adjacent β-sheets. Disruption of this hydrogen bond by Arg mutation to His is predicted to destabilize $\Delta\Delta G$ by 1.7 kcal/mol.

(D) WT and mutant mice were examined for nocifensive withdrawal behavior following stimulation of the trigeminal nerve region in response to mechanical stimulation using a single von Frey filament (#7; 0.6 g). The y axis values represent average responses to three stimulations (on different days; +1 = presence of a stimulus-associated grooming response; −1 = absence of grooming behavior). The Mann-Whitney test was applied to assess statistical difference between WT and mutant mice. A Kruskal-Wallis test evaluated significant differences among all sub-groups: male and female WT and mutants. p value * <0.05; ** <0.01; *** $<1 \times 10^{-3}$; **** $<1 \times 10^{-4}$.

(E and F) Measurement of nociceptive withdrawal threshold using the using the Simplified Up-Down method (SUDO) (Bonin et al., 2014). (E) Graph showing withdrawal threshold results using an adaptation of the method to test in the region innervated by the trigeminal nerve (see Methods; Taylor et al. Pain, 2012). (F) Nociceptive withdrawal threshold in response to mechanical stimulation of the hind paw using calibrated von Frey filaments. p value ** <0.01. See also Figures S1 and S2; Tables S1, S3, S4, and S6; and Videos S1, S2, S3, S4, S5, S6, S7, and S8.

matching the burden of DNMs in the control cohort (Tables S2A and S2B). No genes contained more than one protein-altering DNM (Table S2C). Eleven *de novo* CNVs were identified, including a duplication in *KCNK1*, encoding the inward-rectifying K^+ channel TWIK1 (Table S2D). Of note, pain insensitivity in multiple African rodents has been attributed in part to the down-regulation of *kcnk1* expression (Eigenbrod et al., 2019). No recurrent CNVs were observed.

We performed Gene Ontology (GO) enrichment analysis (Raudvere et al., 2019) of genes harboring damaging DNMs with high brain expression (above 75% percentile among all genes from murine RNA sequencing) (Flegel et al., 2015). Analysis showed the greatest enrichment among genes associated with the molecular function term "GABA receptor binding genes" (GO:0050811) (*GABRG1*, *TRAK1* [Figure 2A]; enrichment = 226.6, adjusted p value = 5.9×10^{-3} [Table S3A]). Damaging DNMs in GO:0050811 genes were enriched in TN cases but not in controls (enrichment = 114.0, p value = 1.5×10^{-4}) (Table S3B). Interestingly, several other notable genes with rare damaging DNMs but not included under the GO term GO:0050811 were identified that, similar to *GABRG1* and *TRAK1*, have elevated brain expression and play important roles in GABA signaling or neurotransmission. These include *ASTN2* (c.1736+2T > C)

(Behesti et al., 2018), *EEF2* (p.Arg839His) (Heise et al., 2017), *UNC80* (p.Lys2794*) (Philippart and Khaliq, 2018; Yeh et al., 2008), and *KIF1B* (p.Arg928Trp) (Aulchenko et al., 2008; Lyons et al., 2009; Zuchner et al., 2004).

GABRG1 encodes the γ-1 subunit of the heteromeric ligand-gated gamma-aminobutyric acid type A receptor ($GABA_AR$) Cl^- channel. Patient TRGN124-1 with iTN-1 had a rare D-mis *GABRG1* DNM (p.Cys188Trp) in a conserved residue of the $GABA_AR$ γ-1 ligand-binding domain that is predicted to disrupt a disulfide bond with Cys202 (ΔΔG = 3.8 kcal/mol) (Figures 2A–2C). Unrelated patient TRGN343-1 with iTN-2 carried a rare D-mis *GABRG1* mutation p.Tyr178His (MAF = 8.2×10^{-6}), which also maps to a conserved residue in the ligand-binding domain and is predicted to disrupt a hydrogen bond between adjacent β-sheets (ΔΔG = 1.7 kcal/mol) (Figures 2A–2C). Another patient with TN in the UK Biobank carried a rare stop-gain mutation in *GABRG1* (p.Trp53*) located just before the ligand-binding domain.

TRAK1 encodes a kinesin adaptor protein that regulates the anterograde axonal transport of mitochondria and $GABA_ARs$ (Barel et al., 2017). Patient TRGN261-1 with iTN-2 had a rare D-mis *TRAK1* DNM (p.Glu798Lys) (Figure S2A) in a conserved residue of the second kinesin-binding Milton domain of *TRAK1* (Figure S2B). Unrelated patient TRGN107-1 with cTN-1 carried the unphased heterozygous D-mis *TRAK1* mutation (p.Arg124Gln) with an MAF just above our threshold (1.6×10^{-5}). p.Arg124Gln maps to a highly conserved residue in the *TRAK1* HAP1_N domain (IPR006933) that directly participates in $GABA_AR$ trafficking in conjunction with kinesin (KIF) proteins (Gilbert et al., 2006). Recessive *TRAK1* mutations cause early infantile epileptic encephalopathy (OMIM# 618201) (Barel et al., 2017), and *Trak1* knockout mice exhibit severely reduced central nervous system (CNS) abundance of $GABA_ARs$ (Gilbert et al., 2006).

A total of nine rare (MAF $\leq 1.0 \times 10^{-5}$) damaging *de novo*, transmitted, or unphased mutations were identified in GO:0050811 GABA receptor-binding genes, yielding enrichment compared with gnomAD controls (odds ratio [OR] = 3.3, one-tailed Fisher's exact p value = 3.8×10^{-3}; Tables S3C and S3D). These genes included $GABA_AR$ subunit α-5 *GABRA5* and trafficking regulators *PLCL1*, *JAKMIP1*, and *ARFGEF2*. Extension of our search to the 21 genes encoding HUGO Gene Nomenclature Committee (HGNC)-designated GABA receptor subunits identified two additional rare, damaging heterozygous mutations in the $GABA_AR$ α-6 and ϵ subunits, *GABRA6* and *GABRE* (Figure S1G). *GABRA5* p.Glu107Gln and *GABRA6* p.Glu90Ala both map to respective ligand-binding domains, whereas *GABRE* p.Trp300* affects the neurotransmitter gating domain (Figures S1H–S1J).

Mouse Model of TN Engineered with a Patient-Specific *GABRG1* Mutation

As proof of principle, we generated a mouse model of one of the identified human TN-associated $GABA_AR$ DNMs (*GABRG1* p.Cys188Trp), using Crispr/CAS9 mutagenesis (Figure S2). To test for trigeminal pain hypersensitivity, we quantified nocifensive behaviors using a modified version of a facial stimulation test (Bailey and Ribeiro-da-Silva, 2006). In contrast to wild-type littermates (n = 23 mice), mutant mice (n = 25) showed significant nocifensive behaviors in response to tactile stimulation of the trigeminal nerve region (Figure 2D; p value < 1×10^{-4}; Mann-Whitney test; Videos S1, S2, S3, S4, S5, S6, S7, and S8 and Table S4A) in both males (n = 11 wild-type and 12 mutants) and females (n = 12 wild-type and 13 mutants; p value = 0.045 for females; p value = 9×10^{-4} for males; Kruskal-Wallis test). No significant difference in nocifensive behavior was observed between male and female mutants (p value = 0.40). To measure nociceptive withdrawal threshold, we also used a modified mechanical threshold test (Bonin et al., 2014; Taylor et al., 2012). Mutant mice (n = 11) showed a significantly lower nociceptive withdrawal threshold than wild-types (n = 9; p value = 1.0×10^{-3}; Mann-Whitney test Figure 2E and Table S4B). Hind paw nociceptive withdrawal threshold was also significantly reduced in mutant mice (p value = 1.6×10^{-3}; Figures 2F and Table S4B).

Significant Burden of Inherited and Unphased *CACNA1H* Variants

Next, we performed burden analysis of rare *de novo* and inherited/unphased variants in 290 TN probands, adjusting for *de novo* mutability using a one-tailed binomial test. Analysis of ultra-rare variants at MAF $\leq 1 \times 10^{-5}$ did not identify significantly enriched genes. However, among moderately rare variants at MAF $\leq 1 \times 10^{-4}$, the Cav3.2 T-type Ca^{2+} channel α-1H subunit (*CACNA1H*) reached genome-wide significant enrichment in cases (enrichment = 3.7, p value = 2.4×10^{-6}; Figure 3A and Table S5A). *CACNA1H* contained 19 predicted damaging variants, including one LoF variant and 18 D-mis variants (Table S5B). Among these, 16 are unphased and 3 are transmitted with incomplete penetrance. The *CACNA1H* variants

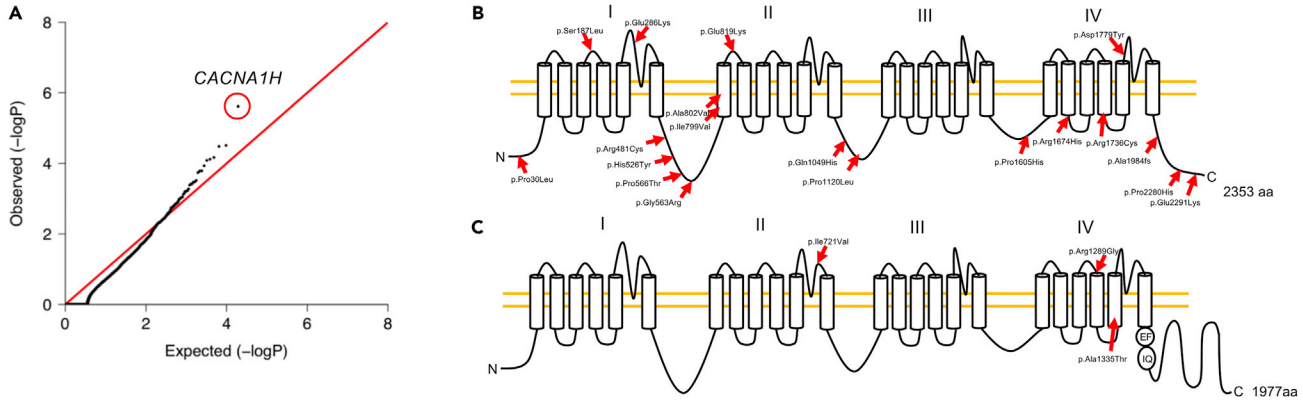

Figure 3. Gene Burden Analysis for Heterozygous Damaging Mutations and Mutation Mapping in Ca^{2+} Channels Encoded by *CACNA1H* and *CACNA1F*

(A) Quantile-quantile plot of observed versus expected p values for damaging (LoF and D-mis) variants with MAF $\leq 1 \times 10^{-4}$. The genome-wide significant gene *CACNA1H* is circled in red. The genome significance cutoff is 2.6×10^{-6}, 0.05/19,347.

(B and C) Mutation mapping of (B) CACNA1H and (C) CACNA1F. CACNA1H graph was adapted from Rzhepetskyy et al. (Rzhepetskyy et al., 2016); CACNA1F graph was modified from (Haeseleer et al., 2016).

See also Figure S3 and Table S5.

map to extracellular, intracellular, and intra-membrane regions of the ion channel (Figure 3B) and are predicted to impact Cav3.2 protein structure (Figures S3A–S3N). In one family, the *CACNA1H* D-mis variant p.Arg1674His was shared by proband TRGN282-1 and his sister TRGN282-2, both similarly affected by medically intractable iTN1.

Identification of Hemizygous Variants in *CACNA1F*

Lastly, we examined recessive and hemizygous genotypes. No genes harbored more than one recessive genotype in 249 TN probands. However, case-control analysis comparing rare damaging hemizygous variants (MAF $\leq 5 \times 10^{-5}$) in 49 male TN probands with male controls in gnomAD identified *CACNA1F*, encoding the Cav3.2 T-type Ca^{2+} channel α-1H subunit, as the most significantly enriched gene (OR = 12.0, p value = 2.43×10^{-3}; Table S5C). *CACNA1F* contained three rare D-mis variants (Figure 3C and Table S5D). p.Ala1335Thr and pArg1289Gly, respectively, mapped to the exofacial and endofacial surfaces of the channel. p.Ile721Val mapped to an extracellular loop of the channel. All three variants are predicted to significantly impact *CACNA1F* channel structure (Figures S3O–S3T).

DISCUSSION

These results provide insight into the genomic architecture of TN. We ascertained the largest collection of familial forms of TN to date and identified several candidate genes with mutational enrichment in TN probands. Our findings implicate *de novo* and inherited rare, damaging variants in GABA signaling and other ion transport genes in TN pathogenesis in a subset of patients. Our creation of a knock-in mouse with the TN-associated *de novo GABRG1* p.Cys188Trp mutation represents an important attempt to engineer a TN animal model with a human mutation.

Previous candidate gene sequencing approaches had identified *SCN8A* and *SLC6A4* as potential TN-associated genes (Cui et al., 2014; Tanaka et al., 2016). In our WES study, we detected only two rare transmitted mutations in *SCN8A* and none in *SLC6A4*. Nonetheless, our data implicate other ion transport pathways in the genetic architecture of TN, including genes related to the function of the ligand-gated $GABA_AR$ Cl^- channel. These findings are consistent with the expression of $GABA_ARs$ along sensory axons (Bhisitkul et al., 1990; Oyelese et al., 1997), with the well-documented role of $GABA_AR$ signaling in trigeminal pathway nociception (Dieb and Hafidi, 2015; Jang et al., 2017; Kaushal et al., 2016; Martin et al., 2010; Wei et al., 2013), with the efficacy of GABA-modulating drugs in some patients with TN (Granger et al., 1995; White et al., 2000) (Table S6), and with the established importance of $GABA_AR$ disinhibition and consequent neuronal hyperexcitability in neuropathic pain (Dieb and Hafidi, 2015; Jang et al., 2017; Martin et al., 2010). These observations support our speculation that frequent co-occurrence of anxiety, depression, and other psychiatric conditions with TN, especially those in younger patients (Mousavi et al., 2016) (often

unresponsive to MVD) (Hamlyn, 1997a), may reflect pleiotropy of germline variants impacting other aspects of GABA signaling.

In addition to variants in GABA signaling genes, we also identified rare dominant variants in the *SCN8A*-related Nav1.5 Na^+ channel gene *SCN5A* in two multiplex TN families, a genome-wide significant enrichment of rare dominant variants in the $Ca_v3.2$ α-1H subunit *CACNA1H* and multiple rare X-linked hemizygous variants in the related $Ca_v3.2$ α-1F subunit *CACNA1F*. Not only are *SCN5A* mutations well known to cause cardiac rhythm disorders including long QT syndrome subtype 3, Brugada syndrome, and cardiac conduction disease (Zimmer and Surber, 2008), but they are also expressed in the brain (Kerr et al., 2004) and have been implicated in both epilepsy (Parisi et al., 2013) and schizophrenia (Roberts, 2006). *CACNA1H* variants have been previously implicated in congenital pain (Souza et al., 2016) and epilepsy (Eckle et al., 2014). T-type Ca^{2+} currents mediated by $Ca_v3.2$/α-1H are activated during $GABA_AR$-mediated depolarizations and subsequently trigger action potential in sensory neurons (Aptel et al., 2007) and mechanosensation in nerve root ganglia (Shin et al., 2003). Increased expression of $Ca_v3.2$ in damaged dorsal root ganglion neurons contributes to the development of neuropathic pain triggered by spared nerve injury (Kang et al., 2018). The closely-related $Ca_v3.1$ has been shown to be a key element in the pathophysiology of a mouse model of trigeminal neuropathic pain (Choi et al., 2016). Mechanical thresholds of pain are significantly altered in a rat model of congenital stationary night blindness with a *Cacna1f* mutation (An et al., 2012). Detailed electrophysiology of these TN-associated *SCN5A*, *CACNA1H*, and *CACNA1F* channel variants in cell culture systems and animal models will be rich topics for future investigation.

How might these mutations and other gene variants contribute to TN pathology? One possibility is a "genetic-mechanical" model, in which a germline mutation confers increased sensitivity to the trigeminal ganglia or axons to NVC by an offending blood vessel, such as the superior cerebellar artery in the cerebello-pontine angle. This mechanism may contribute to unilaterality of symptoms in some patients with NVC and has been proposed for a gain-of-function mutation in *SCN8A* (Tanaka et al., 2016). A germline mutation could also predispose patients to the development of bilateral symptoms, as is seen in some patients with TN. Alternatively, a germline mutation could predispose an individual to later-onset TN arising from a second somatic mutation in the other allele of the same, or another, gene, in trigeminal ganglion neurons or other downstream brainstem or thalamo-cortical projection neurons in the trigeminal system circuitry. Such a "two-hit" model has been seen in other neurovascular cutaneous syndromes with unilateral or multifocal lesions (Brouillard et al., 2002; Pagenstecher et al., 2009; Revencu et al., 2013).

Our data suggest that rare, damaging exonic variants with large effect likely contribute to the pathogenesis of a small fraction of TN cases. Nonetheless, the investigation of such rare variants, especially DNMs, is a proven strategy to gain insight into disease pathogenesis. Therefore, continued gene discovery and functional analysis, including mechanistic work and drug screening in humanized animal models such as our *GABRG1* p.Cys188Trp knock-in mouse, could further elucidate TN pathophysiology, improve diagnostics, and optimally stratify certain patients for specific treatments (e.g., a GABA-modulating drug instead of a craniotomy for MVD). Moreover, the identification of rare, damaging mutations with large effect (even in single patients) has the potential to identify unexpected targets for the development of non-addictive analgesics that could have broader relevance for other neuropathic pain syndromes (Yekkirala et al., 2017). Our findings suggest a WES approach might also be suitable to study hemifacial spasm, another cranial nerve pain syndrome with known familial occurrences that has been classically attributed to NVC and treated with neurosurgical MVD (Campbell and Keedy, 1947; Carter et al., 1990; Coad et al., 1991; Friedman et al., 1989; Haller et al., 2016; Lagalla et al., 2010; Miwa et al., 2002).

Limitations of the Study

A limitation of our study, necessary given our article's genomic focus and the magnitude of the effort, time, and expense required for patient recruitment, phenotyping, and bioinformatic analysis, is our lack of functional and mechanistic follow-up. In future work, the functional consequences of the identified mutations on channel or protein function using electrophysiological techniques in heterologous expression systems, or even better, model organisms with engineered patient mutations (starting with our *GABRG1* mutant mouse), will be required. In these models, it will be important to establish the effect of mutated proteins on trigeminal pain circuitry; the expression of some our mutated proteins in second- or higher-order neurons of the trigeminal nucleus suggests that CNS defects might contribute to pathology. Our current genomics article sets a foundation for these detailed functional studies.

Another limitation of our study is its focus on the role of rare coding variants. Given the impact of common variants in multiple neuropathic pain disorders (Gormley et al., 2018; Meng et al., 2015a, 2015b), we examined the contribution to TN from common variants through a genome-wide association analysis of 236 European cases and 348,028 ethnicity-matching controls from the UK Biobank. No common variants reached genome-wide significance (Figures S4A and S4B). However, the small number of available cases limited the power of our analysis. A power calculation suggests that ~1,600 cases are needed to achieve 80% power assuming moderate effect size ($\lambda = 1.3$) and an MAF of 0.2 for risk alleles (Figure S4C). Our analysis for these variants is thus underpowered. Future studies examining common variants will require a greater numbers of TN probands.

Although childhood and adolescent onset of TN has been reported (Bahgat et al., 2011), the high prevalence of TN and its inconsistent segregation patterns within families suggests that complex epistatic interactions, gene-environment interactions, or effects from common polygenic variants could also play important pathogenic roles in TN (Gormley et al., 2018; Zorina-Lichtenwalter et al., 2018). Addressing these questions will be important and challenging topics of future investigations.

Resource Availability

Lead Contact

Further information and requests for resources and reagents should be directed to and will be fulfilled by the Lead Contact (kristopher.kahle@yale.edu).

Materials Availability

No plasmids were generated in this study. Mouse lines generated in this study will be deposited to the Knockout Mouse Project (KOMP) and are available upon request.

Data and Code Availability

The WES data generated during this study are available at dbGap with accession number phs000744. Original data for the mouse experiments in Figures 2D–2F in the article are available at Table S4. Our in-house Python and R pipelines are available from the corresponding author on request.

METHODS

All methods can be found in the accompanying Transparent Methods supplemental file.

SUPPLEMENTAL INFORMATION

Supplemental Information can be found online at https://doi.org/10.1016/j.isci.2020.101552.

ACKNOWLEDGMENTS

We thank the patients and families who participated in this research. We acknowledge Dr. Hongyu Zhao from the Department of Biostatistics, Yale School of Public Health for his mentorship on the statistical analysis and providing access to the UK Biobank Resource under Application Number 29900. We acknowledge support from the Yale-NIH Center for Mendelian Genomics (5U54HG006504) and an NIH NRCDP award to K.T.K. We acknowledge the Canadian Institute of Health Research (CIHR) Foundation grant (FDN389050) to Y.D.K. and CIHR grant (MOP-111072 and MOP-130373) to M.C. We acknowledge Dr. Kaya Bilguvar for his help on exome sequencing for the samples at Yale-NIH Center for Mendelian Genomics. W.D. was supported by American Heart Association Predoctoral Fellowship (19PRE34380842). S.C.J. was supported by the James Hudson Brown-Alexander Brown Coxe Postdoctoral Fellowship, the American Heart Association Postdoctoral Fellowship (18POST34060008), and the K99/R00 Pathway to Independence Award (K99HL143036 and R00HL143036-02). Y.D.K. was supported by a Canada Research Chair in Chronic Pain and Related Brain Disorders.

AUTHOR CONTRIBUTIONS

Study design and conceptualization: W.D., R.P.L., and K.T.K. Cohort ascertainment, recruitment, and phenotypic characterization: A.A., S.P., J.H., A.S., J.G., A.D., C.G.F., and S.C. Exome sequencing production and validation: S.M., C.C., F.L.-G., and J.R.K. WES analysis: W.D., S.C.J., X.Z., A.H.S., J.C., and M.C.S. Statistical analysis: W.D., S.C.J., A.H.S., S.P., B.L., Q.L., G.Z., W.L., and X.L. Mouse experiments: A.C.,

L.-E.L., G.B., K.B., and Y.D.K. Sanger sequencing validation: C.N.-W. Biophysical simulation: B.I. and S.H. Resources: R.P.L., and K.T.K. Writing and review of manuscript: W.D., S.C.J., A.A., S.P., A.H.S., E.K., P.Q.D., A.J.K., R.F.S., J.M.S., E.N.E., C.G., J.M., M.G., J.L.G., S.D.-H., S.G.W., F.G.B., S.L.A., M.C., R.P.L., and K.T.K. Project administration: W.D., E.L., Y.D.K., R.P.L., and K.T.K. Funding acquisition and supervision: R.P.L. and K.T.K.

DECLARATION OF INTERESTS

The authors declare no competing interests.

Received: June 18, 2020
Revised: September 6, 2020
Accepted: September 8, 2020
Published: October 23, 2020

REFERENCES

Ackerman, M.J., Siu, B.L., Sturner, W.Q., Tester, D.J., Valdivia, C.R., Makielski, J.C., and Towbin, J.A. (2001). Postmortem molecular analysis of SCN5A defects in sudden infant death syndrome. JAMA *286*, 2264–2269.

Ahmed, O.L., Akinyele, O.A., Akindayo, A.O., and Bamidele, K. (2012). Management of trigeminal neuralgia using amitriptyline and pregablin combination therapy. Afr. J. Biomed. Res. *15*, 201–203.

Al-Quliti, K.W. (2015). Update on neuropathic pain treatment for trigeminal neuralgia. The pharmacological and surgical options. Neurosciences (Riyadh) *20*, 107–114.

Allen, A.S., Berkovic, S.F., Cossette, P., Delanty, N., Dlugos, D., Eichler, E.E., Epstein, M.P., Glauser, T., Goldstein, D.B., Han, Y., et al. (2013). De novo mutations in epileptic encephalopathies. Nature *501*, 217–221.

Alter, B.J., Zhao, C., Karim, F., Landreth, G.E., and Gereau, R.W.t. (2010). Genetic targeting of ERK1 suggests a predominant role for ERK2 in murine pain models. J. Neurosci. *30*, 11537–11547.

An, J., Wang, L., Guo, Q., Li, L., Xia, F., and Zhang, Z. (2012). Behavioral phenotypic properties of a natural occurring rat model of congenital stationary night blindness with Cacna1f mutation. J. Neurogenet. *26*, 363–373.

Aptel, H., Hilaire, C., Pieraut, S., Boukhaddaoui, H., Mallie, S., Valmier, J., and Scamps, F. (2007). The Cav3.2/alpha1H T-type Ca2+ current is a molecular determinant of excitatory effects of GABA in adult sensory neurons. Mol. Cell Neurosci. *36*, 293–303.

Aulchenko, Y.S., Hoppenbrouwers, I.A., Ramagopalan, S.V., Broer, L., Jafari, N., Hillert, J., Link, J., Lundstrom, W., Greiner, E., Dessa Sadovnick, A., et al. (2008). Genetic variation in the KIF1B locus influences susceptibility to multiple sclerosis. Nat. Genet. *40*, 1402–1403.

Bahgat, D., Ray, D.K., Raslan, A.M., McCartney, S., and Burchiel, K.J. (2011). Trigeminal neuralgia in young adults. J. Neurosurg. *114*, 1306–1311.

Bailey, A.L., and Ribeiro-da-Silva, A. (2006). Transient loss of terminals from non-peptidergic nociceptive fibers in the substantia gelatinosa of spinal cord following chronic constriction injury of the sciatic nerve. Neuroscience *138*, 675–690.

Barel, O., Malicdan, M.C.V., Ben-Zeev, B., Kandel, J., Pri-Chen, H., Stephen, J., Castro, I.G., Metz, J., Atawa, O., Moshkovitz, S., et al. (2017). Deleterious variants in TRAK1 disrupt mitochondrial movement and cause fatal encephalopathy. Brain *140*, 568–581.

Behesti, H., Fore, T.R., Wu, P., Horn, Z., Leppert, M., Hull, C., and Hatten, M.E. (2018). ASTN2 modulates synaptic strength by trafficking and degradation of surface proteins. Proc. Natl. Acad. Sci. U S A *115*, E9717–E9726.

Bhisitkul, R.B., Kocsis, J.D., Gordon, T.R., and Waxman, S.G. (1990). Trophic influence of the distal nerve segment on GABAA receptor expression in axotomized adult sensory neurons. Exp. Neurol. *109*, 273–278.

Bonin, R.P., Bories, C., and De Koninck, Y. (2014). A simplified up-down method (SUDO) for measuring mechanical nociception in rodents using von Frey filaments. Mol. Pain *10*, 26.

Brisman, R. (1987). Bilateral trigeminal neuralgia. J. Neurosurg. *67*, 44–48.

Brouillard, P., Boon, L.M., Mulliken, J.B., Enjolras, O., Ghassibe, M., Warman, M.L., Tan, O.T., Olsen, B.R., and Vikkula, M. (2002). Mutations in a novel factor, glomulin, are responsible for glomuvenous malformations ("glomangiomas"). Am. J. Hum. Genet. *70*, 866–874.

Burchiel, K.J. (1980a). Abnormal impulse generation in focally demyelinated trigeminal roots. J. Neurosurg. *53*, 674–683.

Burchiel, K.J. (1980b). Ectopic impulse generation in focally demyelinated trigeminal nerve. Exp. Neurol. *69*, 423–429.

Burchiel, K.J., and Baumann, T.K. (2004). Pathophysiology of trigeminal neuralgia: new evidence from a trigeminal ganglion intraoperative microneurographic recording. J. Neurosurg. *101*, 872–873.

Campbell, E., and Keedy, C. (1947). Hemifacial spasm; a note on the etiology in two cases. J. Neurosurg. *4*, 342–347.

Carter, J.B., Patrinely, J.R., Jankovic, J., McCrary, J.A., 3rd, and Boniuk, M. (1990). Familial hemifacial spasm. Arch. Ophthalmol. *108*, 249–250.

Choi, S., Yu, E., Hwang, E., and Llinas, R.R. (2016). Pathophysiological implication of CaV3.1 T-type Ca2+ channels in trigeminal neuropathic pain. Proc. Natl. Acad. Sci. U S A *113*, 2270–2275.

Coad, J.E., Wirtschafter, J.D., Haines, S.J., Heros, R.C., and Perrone, T. (1991). Familial hemifacial spasm associated with arterial compression of the facial nerve. J. Neurosurg. *74*, 290–296.

Cruccu, G., Finnerup, N.B., Jensen, T.S., Scholz, J., Sindou, M., Svensson, P., Treede, R.D., Zakrzewska, J.M., and Nurmikko, T. (2016). Trigeminal neuralgia: new classification and diagnostic grading for practice and research. Neurology *87*, 220–228.

Cui, W., Yu, X., and Zhang, H. (2014). The serotonin transporter gene polymorphism is associated with the susceptibility and the pain severity in idiopathic trigeminal neuralgia patients. J. Headache Pain *15*, 42.

Devor, M., Amir, R., and Rappaport, Z.H. (2002). Pathophysiology of trigeminal neuralgia: the ignition hypothesis. Clin. J. Pain *18*, 4–13.

Dieb, W., and Hafidi, A. (2015). Mechanism of GABA involvement in post-traumatic trigeminal neuropathic pain: activation of neuronal circuitry composed of PKCgamma interneurons and pERK1/2 expressing neurons. Eur. J. Pain *19*, 85–96.

Dong, C., Wei, P., Jian, X., Gibbs, R., Boerwinkle, E., Wang, K., and Liu, X. (2015). Comparison and integration of deleteriousness prediction methods for nonsynonymous SNVs in whole exome sequencing studies. Hum. Mol. Genet. *24*, 2125–2137.

Duran, D., Zeng, X., Jin, S.C., Choi, J., Nelson-Williams, C., Yatsula, B., Gaillard, J., Furey, C.G., Lu, Q., Timberlake, A.T., et al. (2019). Mutations in chromatin modifier and ephrin signaling genes in vein of galen malformation. Neuron *101*, 429–443 e424.

Eckle, V.S., Shcheglovitov, A., Vitko, I., Dey, D., Yap, C.C., Winckler, B., Perez-Reyes, E., and Perez-Reyes, E. (2014). Mechanisms by which a

CACNA1H mutation in epilepsy patients increases seizure susceptibility. J. Physiol. *592*, 795–809.

Eigenbrod, O., Debus, K.Y., Reznick, J., Bennett, N.C., Sanchez-Carranza, O., Omerbasic, D., Hart, D.W., Barker, A.J., Zhong, W., Lutermann, H., et al. (2019). Rapid molecular evolution of pain insensitivity in multiple African rodents. Science *364*, 852–859.

Fleetwood, I.G., Innes, A.M., Hansen, S.R., and Steinberg, G.K. (2001). Familial trigeminal neuralgia. Case report and review of the literature. J. Neurosurg. *95*, 513–517.

Flegel, C., Schobel, N., Altmuller, J., Becker, C., Tannapfel, A., Hatt, H., and Gisselmann, G. (2015). RNA-seq analysis of human trigeminal and dorsal root ganglia with a focus on chemoreceptors. PLoS One *10*, e0128951.

Friedman, A., Jamrozik, Z., and Bojakowski, J. (1989). Familial hemifacial spasm. Mov. Disord. *4*, 213–218.

Furey, C.G., Choi, J., Jin, S.C., Zeng, X., Timberlake, A.T., Nelson-Williams, C., Mansuri, M.S., Lu, Q., Duran, D., Panchagnula, S., et al. (2018). De novo mutation in genes regulating neural Stem cell fate in human congenital hydrocephalus. Neuron *99*, 302–314 e304.

Gardner, W.J., and Miklos, M.V. (1959). Response of trigeminal neuralgia to decompression of sensory root; discussion of cause of trigeminal neuralgia. J. Am. Med. Assoc. *170*, 1773–1776.

Gilbert, S.L., Zhang, L., Forster, M.L., Anderson, J.R., Iwase, T., Soliven, B., Donahue, L.R., Sweet, H.O., Bronson, R.T., Davisson, M.T., et al. (2006). Trak1 mutation disrupts GABA(A) receptor homeostasis in hypertonic mice. Nat. Genet. *38*, 245–250.

Gormley, P., Kurki, M.I., Hiekkala, M.E., Veerapen, K., Happola, P., Mitchell, A.A., Lal, D., Palta, P., Surakka, I., Kaunisto, M.A., et al. (2018). Common variant burden contributes to the familial aggregation of migraine in 1,589 families. Neuron *99*, 1098.

Granger, P., Biton, B., Faure, C., Vige, X., Depoortere, H., Graham, D., Langer, S.Z., Scatton, B., and Avenet, P. (1995). Modulation of the gamma-aminobutyric acid type A receptor by the antiepileptic drugs carbamazepine and phenytoin. Mol. Pharmacol. *47*, 1189–1196.

Haeseleer, F., Williams, B., and Lee, A. (2016). Characterization of C-terminal Splice variants of Cav1.4 Ca2+ channels in human retina. J. Biol. Chem. *291*, 15663–15673.

Haines, S.J., Jannetta, P.J., and Zorub, D.S. (1980). Microvascular relations of the trigeminal nerve. An anatomical study with clinical correlation. J. Neurosurg. *52*, 381–386.

Haller, S., Etienne, L., Kovari, E., Varoquaux, A.D., Urbach, H., and Becker, M. (2016). Imaging of neurovascular compression syndromes: trigeminal neuralgia, hemifacial spasm, vestibular paroxysmia, and glossopharyngeal neuralgia. Am. J. Neuroradiol. *37*, 1384–1392.

Hamlyn, P.J. (1997a). Neurovascular relationships in the posterior cranial fossa, with special reference to trigeminal neuralgia. 1. Review of the literature and development of a new method of vascular injection-filling in cadaveric controls. Clin. Anat. *10*, 371–379.

Hamlyn, P.J. (1997b). Neurovascular relationships in the posterior cranial fossa, with special reference to trigeminal neuralgia. 2. Neurovascular compression of the trigeminal nerve in cadaveric controls and patients with trigeminal neuralgia: quantification and influence of method. Clin. Anat. *10*, 380–388.

Harris, W. (1936). Bilateral trigeminal tic: its association with heredity and disseminated sclerosis. Ann. Surg. *103*, 161–172.

Headache Classification Committee of the International Headache Society (IHS) (2013). The international classification of Headache disorders, 3rd edition (beta version). Cephalalgia *33*, 629–808.

Heise, C., Taha, E., Murru, L., Ponzoni, L., Cattaneo, A., Guarnieri, F.C., Montani, C., Mossa, A., Vezzoli, E., Ippolito, G., et al. (2017). eEF2K/eEF2 pathway controls the excitation/inhibition balance and susceptibility to epileptic Seizures. Cereb. Cortex *27*, 2226–2248.

Hilton, D.A., Love, S., Gradidge, T., and Coakham, H.B. (1994). Pathological findings associated with trigeminal neuralgia caused by vascular compression. Neurosurgery *35*, 299–303, discussion 303.

Hocking, L.J., Generation, S., Morris, A.D., Dominiczak, A.F., Porteous, D.J., and Smith, B.H. (2012). Heritability of chronic pain in 2195 extended families. Eur. J. Pain *16*, 1053–1063.

Hughes, M.A., Jani, R.H., Fakhran, S., Chang, Y.F., Branstetter, B.F., Thirumala, P.D., and Sekula, R.F. (2019). Significance of degree of neurovascular compression in surgery for trigeminal neuralgia. J. Neurosurg. *133*, 411–416.

Iossifov, I., Ronemus, M., Levy, D., Wang, Z., Hakker, I., Rosenbaum, J., Yamrom, B., Lee, Y.H., Narzisi, G., Leotta, A., et al. (2012). De novo gene disruptions in children on the autistic spectrum. Neuron *74*, 285–299.

Jang, I.J., Davies, A.J., Akimoto, N., Back, S.K., Lee, P.R., Na, H.S., Furue, H., Jung, S.J., Kim, Y.H., and Oh, S.B. (2017). Acute inflammation reveals GABAA receptor-mediated nociception in mouse dorsal root ganglion neurons via PGE2 receptor 4 signaling. Physiol. Rep. *5*, e13178.

Jani, R.H., Hughes, M.A., Gold, M.S., Branstetter, B.F., Ligus, Z.E., and Sekula, R.F., Jr. (2019). Trigeminal nerve compression without trigeminal neuralgia: intraoperative vs imaging evidence. Neurosurgery *84*, 60–65.

Jin, S.C., Homsy, J., Zaidi, S., Lu, Q., Morton, S., DePalma, S.R., Zeng, X., Qi, H., Chang, W., Sierant, M.C., et al. (2017). Contribution of rare inherited and de novo variants in 2,871 congenital heart disease probands. Nat. Genet. *49*, 1593–1601.

Kang, X.J., Chi, Y.N., Chen, W., Liu, F.Y., Cui, S., Liao, F.F., Cai, J., and Wan, Y. (2018). Increased expression of CaV3.2 T-type calcium channels in damaged DRG neurons contributes to neuropathic pain in rats with spared nerve injury. Mol. Pain *14*, 1744806918765808.

Katusic, S., Williams, D.B., Beard, C.M., Bergstralh, E.J., and Kurland, L.T. (1991). Epidemiology and clinical features of idiopathic trigeminal neuralgia and glossopharyngeal neuralgia: similarities and differences, Rochester, Minnesota, 1945-1984. Neuroepidemiology *10*, 276–281.

Kaushal, R., Taylor, B.K., Jamal, A.B., Zhang, L., Ma, F., Donahue, R., and Westlund, K.N. (2016). GABA-A receptor activity in the noradrenergic locus coeruleus drives trigeminal neuropathic pain in the rat; contribution of NAalpha1 receptors in the medial prefrontal cortex. Neuroscience *334*, 148–159.

Kerr, N.C., Holmes, F.E., and Wynick, D. (2004). Novel isoforms of the sodium channels Nav1.8 and Nav1.5 are produced by a conserved mechanism in mouse and rat. J. Biol. Chem. *279*, 24826–24833.

Kircher, M., Witten, D.M., Jain, P., O'Roak, B.J., Cooper, G.M., and Shendure, J. (2014). A general framework for estimating the relative pathogenicity of human genetic variants. Nat. Genet. *46*, 310–315.

Lagalla, G., Logullo, F., Di Bella, P., Haghighipour, R., and Provinciali, L. (2010). Familial hemifacial spasm and determinants of late onset. Neurol. Sci. *31*, 17–22.

Liverman, C.S., Brown, J.W., Sandhir, R., Klein, R.M., McCarson, K., and Berman, N.E. (2009). Oestrogen increases nociception through ERK activation in the trigeminal ganglion: evidence for a peripheral mechanism of allodynia. Cephalalgia *29*, 520–531.

Lyons, D.A., Naylor, S.G., Scholze, A., and Talbot, W.S. (2009). Kif1b is essential for mRNA localization in oligodendrocytes and development of myelinated axons. Nat. Genet. *41*, 854–858.

Maarbjerg, S., Wolfram, F., Gozalov, A., Olesen, J., and Bendtsen, L. (2015). Significance of neurovascular contact in classical trigeminal neuralgia. Brain *138*, 311–319.

Maarbjerg, S., Di Stefano, G., Bendtsen, L., and Cruccu, G. (2017). Trigeminal neuralgia - diagnosis and treatment. Cephalalgia *37*, 648–657.

MacDonald, B.K., Cockerell, O.C., Sander, J.W., and Shorvon, S.D. (2000). The incidence and lifetime prevalence of neurological disorders in a prospective community-based study in the UK. Brain *123* (Pt 4), 665–676.

Martin, Y.B., Malmierca, E., Avendano, C., and Nunez, A. (2010). Neuronal disinhibition in the trigeminal nucleus caudalis in a model of chronic neuropathic pain. Eur. J. Neurosci. *32*, 399–408.

Meng, W., Deshmukh, H.A., Donnelly, L.A., Wellcome Trust Case Control Consortium 2, Surrogate Markers for Micro and Macro-Vascular Hard Endpoints for Innovative Diabetes Tools Study Group, Torrance, N., Colhoun, H.M., Palmer, C.N., and Smith, B.H. (2015a). A genome-wide association study provides evidence of Sex-specific involvement of Chr1p35.1 (ZSCAN20-TLR12P) and Chr8p23.1 (HMGB1P46) with diabetic neuropathic pain. EBioMedicine *2*, 1386–1393.

Meng, W., Deshmukh, H.A., van Zuydam, N.R., Liu, Y., Donnelly, L.A., Zhou, K., Wellcome Trust Case Control Consortium 2, Surrogate Markers for Micro and Macro-Vascular Hard Endpoints for Innovative Diabetes Tools Study Group, Morris, A.D., Holhuan, H.M., et al. (2015b). A genome-wide association study suggests an association of Chr8p21.3 (GFRA2) with diabetic neuropathic pain. Eur. J. Pain *19*, 392–399.

Miwa, H., Mizuno, Y., and Kondo, T. (2002). Familial hemifacial spasm: report of cases and review of literature. J. Neurol. Sci. *193*, 97–102.

Mousavi, S.H., Sekula, R.F., Gildengers, A., Gardner, P., and Lunsford, L.D. (2016). Concomitant depression and anxiety negatively affect pain outcomes in surgically managed young patients with trigeminal neuralgia: long-term clinical outcome. Surg. Neurol. Int. *7*, 98.

Nielsen, C.S., Knudsen, G.P., and Steingrimsdottir, O.A. (2012). Twin studies of pain. Clin. Genet. *82*, 331–340.

El Otmani, H., Moutaouakil, F., Fadel, H., and Slassi, I. (2008). [Familial trigeminal neuralgia]. Rev. Neurol. (Paris) *164*, 384–387.

Oyelese, A.A., Rizzo, M.A., Waxman, S.G., and Kocsis, J.D. (1997). Differential effects of NGF and BDNF on axotomy-induced changes in GABA(A)-receptor-mediated conductance and sodium currents in cutaneous afferent neurons. J. Neurophysiol. *78*, 31–42.

Pagenstecher, A., Stahl, S., Sure, U., and Felbor, U. (2009). A two-hit mechanism causes cerebral cavernous malformations: complete inactivation of CCM1, CCM2 or CCM3 in affected endothelial cells. Hum. Mol. Genet. *18*, 911–918.

Parisi, P., Oliva, A., Coll Vidal, M., Partemi, S., Campuzano, O., Iglesias, A., Pisani, D., Pascali, V.L., Paolino, M.C., Villa, M.P., et al. (2013). Coexistence of epilepsy and Brugada syndrome in a family with SCN5A mutation. Epilepsy Res. *105*, 415–418.

Philippart, F., and Khaliq, Z.A.-O. (2018). G(i/o) protein-coupled receptors in dopamine neurons inhibit the sodium leak channel NALCN. Elife *7*, e40984.

Pollack, I.F., Jannetta, P.J., and Bissonette, D.J. (1988). Bilateral trigeminal neuralgia: a 14-year experience with microvascular decompression. J. Neurosurg. *68*, 559–565.

The NHLBI Trans-Omics for Precision Medicine (TOPMed) Whole Genome Sequencing Program (2018). BRAVO variant browser: University of Michigan and NHLBI, Available from: https://bravo.sph.umich.edu/freeze5/hg38/.

Rappaport, Z.H., Govrin-Lippmann, R., and Devor, M. (1997). An electron-microscopic analysis of biopsy samples of the trigeminal root taken during microvascular decompressive surgery. Stereotact. Funct. Neurosurg. *68*, 182–186.

Raudvere, U., Kolberg, L., Kuzmin, I., Arak, T., Adler, P., Peterson, H., and Vilo, J. (2019). g:Profiler: a web server for functional enrichment analysis and conversions of gene lists (2019 update). Nucleic Acids Res *47*, W191–W198.

Revencu, N., Boon, L.M., Mendola, A., Cordisco, M.R., Dubois, J., Clapuyt, P., Hammer, F., Amor, D.J., Irvine, A.D., Baselga, E., et al. (2013). RASA1 mutations and associated phenotypes in 68 families with capillary malformation-arteriovenous malformation. Hum. Mutat. *34*, 1632–1641.

Roberts, E. (2006). GABAergic malfunction in the limbic system resulting from an aboriginal genetic defect in voltage-gated Na+-channel SCN5A is proposed to give rise to susceptibility to schizophrenia. Adv. Pharmocol. *54*, 119–145.

Rodriguez, F.B., Simonet, C., Cerdan, D.M., Morollon, N., Guerrero, P., Tabernero, C., and Duarte, J. (2019). Familial classic trigeminal neuralgia. Neurologia *34*, 229–233.

Rzhepetskyy, Y., Lazniewska, J., Blesneac, I., Pamphlett, R., and Weiss, N. (2016). CACNA1H missense mutations associated with amyotrophic lateral sclerosis alter Cav3.2 T-type calcium channel activity and reticular thalamic neuron firing. Channels (Austin) *10*, 466–477.

Shin, J.B., Martinez-Salgado, C., Heppenstall, P.A., and Lewin, G.R. (2003). A T-type calcium channel required for normal function of a mammalian mechanoreceptor. Nat. Neurosci. *6*, 724–730.

Smyth, P., Greenough, G., and Stommel, E. (2003). Familial trigeminal neuralgia: case reports and review of the literature. Headache *43*, 910–915.

Souza, I.A., Gandini, M.A., Wan, M.M., and Zamponi, G.W. (2016). Two heterozygous Cav3.2 channel mutations in a pediatric chronic pain patient: recording condition-dependent biophysical effects. Pflugers Arch. *468*, 635–642.

Sun, S., Sun, J., Jiang, W., Wang, W., and Ni, L. (2019). Nav1.7 via promotion of ERK in the trigeminal ganglion plays an important role in the induction of pulpitis inflammatory pain. Biomed. Res. Int. *2019*, 6973932.

Tanaka, B.S., Zhao, P., Dib-Hajj, F.B., Morisset, V., Tate, S., Waxman, S.G., and Dib-Hajj, S.D. (2016). A gain-of-function mutation in Nav1.6 in a case of trigeminal neuralgia. Mol. Med. *22*, 338–348.

Taylor, A.M., Osikowicz, M., and Ribeiro-da-Silva, A. (2012). Consequences of the ablation of nonpeptidergic afferents in an animal model of trigeminal neuropathic pain. Pain *153*, 1311–1319.

Timberlake, A.T., Choi, J., Zaidi, S., Lu, Q., Nelson-Williams, C., Brooks, E.D., Bilguvar, K., Tikhonova, I., Mane, S., Yang, J.F., et al. (2016). Two locus inheritance of non-syndromic midline craniosynostosis via rare SMAD6 and common BMP2 alleles. Elife *5*, e20125.

Vissers, L.E., de Ligt, J., Gilissen, C., Janssen, I., Steehouwer, M., de Vries, P., van Lier, B., Arts, P., Wieskamp, N., del Rosario, M., et al. (2010). A de novo paradigm for mental retardation. Nat. Genet. *42*, 1109–1112.

Wei, B., Kumada, T., Furukawa, T., Inoue, K., Watanabe, M., Sato, K., and Fukuda, A. (2013). Pre- and post-synaptic switches of GABA actions associated with Cl- homeostatic changes are induced in the spinal nucleus of the trigeminal nerve in a rat model of trigeminal neuropathic pain. Neuroscience *228*, 334–348.

White, H.S., Brown, S.D., Woodhead, J.H., Skeen, G.A., and Wolf, H.H. (2000). Topiramate modulates GABA-evoked currents in murine cortical neurons by a nonbenzodiazepine mechanism. Epilepsia *41*, S17–S20.

Yeh, E., Ng, S., Zhang, M., Bouhours, M., Wang, Y., Wang, M., Hung, W., Aoyagi, K., Melnik-Martinez, K., Li, M., et al. (2008). A putative cation channel, NCA-1, and a novel protein, UNC-80, transmit neuronal activity in C. elegans. PLoS Biol. *6*, e55.

Yekkirala, A.S., Roberson, D.P., Bean, B.P., and Woolf, C.J. (2017). Breaking barriers to novel analgesic drug development. Nat. Rev. Drug Discov. *16*, 545–564.

Zaidi, S., Choi, M., Wakimoto, H., Ma, L., Jiang, J., Overton, J.D., Romano-Adesman, A., Bjornson, R.D., Breitbart, R.E., Brown, K.K., et al. (2013). De novo mutations in histone-modifying genes in congenital heart disease. Nature *498*, 220–223.

Zakrzewska, J.M., and Akram, H. (2011). Neurosurgical interventions for the treatment of classical trigeminal neuralgia. Cochrane Database Syst. Rev., CD007312.

Zimmer, T., and Surber, R. (2008). SCN5A channelopathies–an update on mutations and mechanisms. Prog. Biophys. Mol. Biol. *98*, 120–136.

Zorina-Lichtenwalter, K., Parisien, M., and Diatchenko, L. (2018). Genetic studies of human neuropathic pain conditions: a review. Pain *159*, 583–594.

Zuchner, S., Mersiyanova, I.V., Muglia, M., Bissar-Tadmouri, N., Rochelle, J., Dadali, E.L., Zappia, M., Nelis, E., Patitucci, A., Senderek, J., et al. (2004). Mutations in the mitochondrial GTPase mitofusin 2 cause Charcot-Marie-Tooth neuropathy type 2A. Nat. Genet. *36*, 449–451.

iScience, Volume *23*

Supplemental Information

Exome Sequencing Implicates Impaired GABA Signaling and Neuronal Ion Transport in Trigeminal Neuralgia

Weilai Dong, Sheng Chih Jin, August Allocco, Xue Zeng, Amar H. Sheth, Shreyas Panchagnula, Annie Castonguay, Louis-Étienne Lorenzo, Barira Islam, Geneviève Brindle, Karine Bachand, Jamie Hu, Agata Sularz, Jonathan Gaillard, Jungmin Choi, Ashley Dunbar, Carol Nelson-Williams, Emre Kiziltug, Charuta Gavankar Furey, Sierra Conine, Phan Q. Duy, Adam J. Kundishora, Erin Loring, Boyang Li, Qiongshi Lu, Geyu Zhou, Wei Liu, Xinyue Li, Michael C. Sierant, Shrikant Mane, Christopher Castaldi, Francesc López-Giráldez, James R. Knight, Raymond F. Sekula Jr., J. Marc Simard, Emad N. Eskandar, Christopher Gottschalk, Jennifer Moliterno, Murat Günel, Jason L. Gerrard, Sulayman Dib-Hajj, Stephen G. Waxman, Fred G. Barker II, Seth L. Alper, Mohamed Chahine, Shozeb Haider, Yves De Koninck, Richard P. Lifton, and Kristopher T. Kahle

Figure S1. Mutations in known TN gene *SCN8A*, sodium channel gene *SCN5A, and* GABA receptor subunit genes *GABRA5*, *GABRA6*, and *GABRE*, related to Figure 1,2. (a) Variant information for *SCN8A* p.Arg475Gln and p.Ile1583Thr. (b) SCN8A contains four homologous domains I to IV, each containing 6 transmembrane segments. p.Arg475Gln is located at cytoplasmic loop 1; p.Ile1583Thr mapped to cytoplasmic portion between segment 1 and 2 of the the IV domain. (c) Variant information for *SCN5A* p.Phe1293Ser and p.Arg1826His. (d) Mutation mapping of *SCN5A*. SCN5A contains four homologous domains I to IV, each containing 6 transmembrane segments. p.Phe1293Ser mapped to an extracellular loop of domain III while p.Arg1826His located to the C-terminal cytoplasmic domain. (e) Pedigrees of the two families with inherited *SCN5A* mutations. Sample IDs indicate samples with WES. (f) Modeled structures of regions surrounding wildtype Phe1293 (left) and mutant Phe1293Ser (right). Phe1293 is a conserved residue, positioned in an exofacial hydrophobic pocket between helices S3 and S4, plausibly interacts with the membrane. Mutation to a polar Serine residue would be thermodynamically unfavourable in this hydrophobic environment (ΔΔG = 0.34 kcal/mol). Arg1826His variant could not be modelled due to absence of template. (g) GABRA5, GABRA6 and GABRE each contain a neurotransmitter-gated ion channel ligand-binding domain and a neurotransmitter-gated ion channel transmembrane region. Mutation mapping for (h) GABRA5 p.Glu107Gln and (i) GABRA6 p.Glu90Ala in the ligand binding domain, and (j) GABRE p.Trp300* in the transmembrane region. LBD: ligand-binding domain; Trans: transmembrane region.

a

ID	Mutation type	AA Change	Bravo	MetaSVM	CADD
TRGN136-1	D-mis	p.Ile1583Thr	2.15E-04	D	12.24
2890541	D-mis	p.Arg475Gln	3.27E-04	D	23.3

b

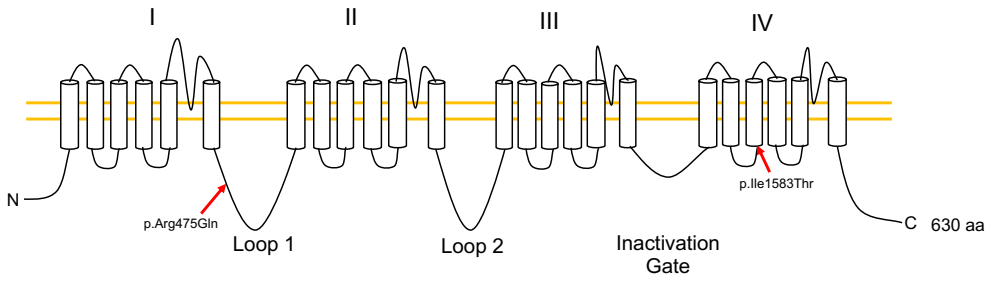

c

Family ID	Mutation type	AA Change	Bravo	MetaSVM	CADD
TRGN141	D-mis	p.Phe1293Ser	2.95E-04	D	23.7
TRGN201	D-mis	p.Arg1826His	1.83E-04	D	34.0

d

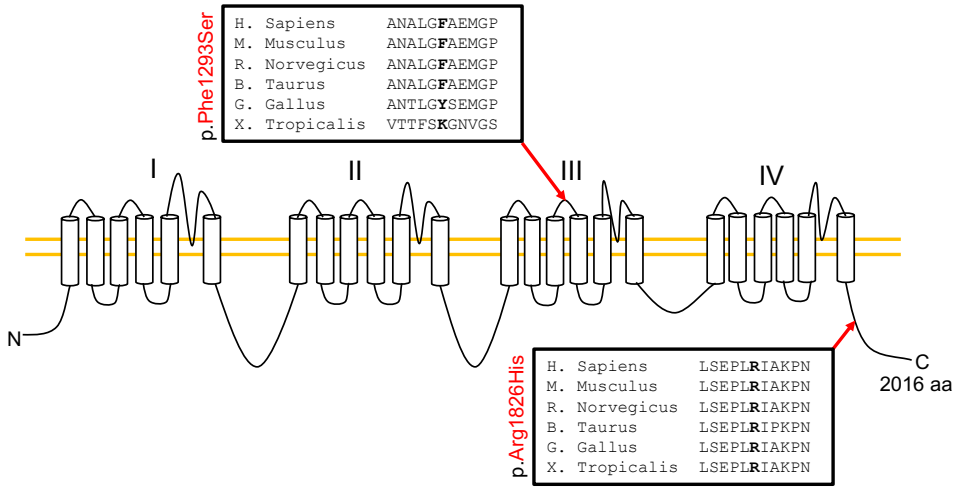

e

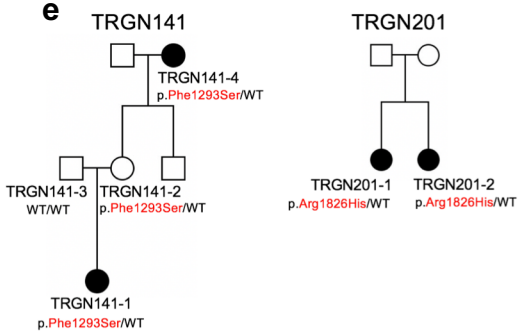

f

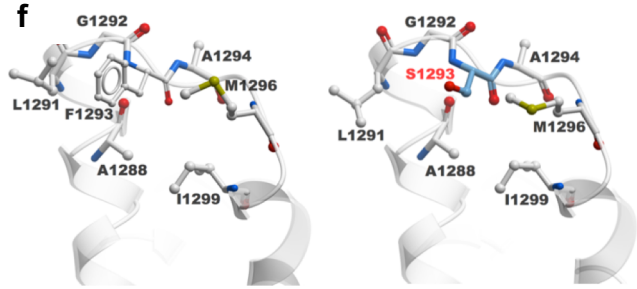

g

ID	Gene	Mutation type	AA Change	Bravo	MetaSVM	CADD
4922269	*GABRA5*	D-mis	p.Glu107Gln	Novel	D	25.3
TRGN107-1	*GABRA6*	D-mis	p.Glu90Ala	Novel	D	25.7
TRGN231-1	*GABRE*	stopgain	p.Trp300*	Novel	NA	42.0

h

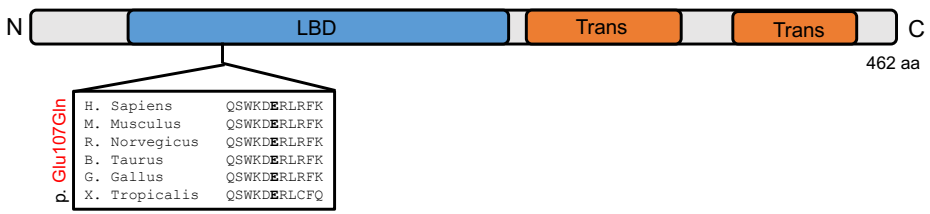

i

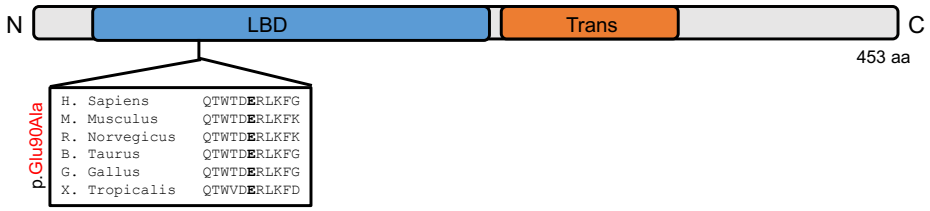

j

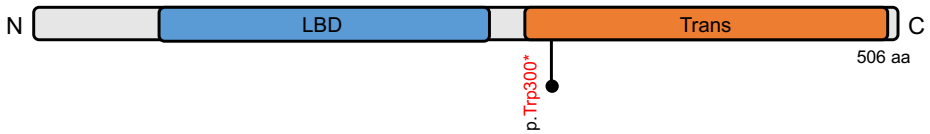

Figure S2. Generation of *Gabrg1* knock-in allele, related to Figure 2. (a) Schematic of the Cas9/sgRNA/oligo-targeting site in exon 5. The 20bp sgRNA coding sequence is in red. The PAM (protospacer adjacent motif) sequence is in green. Four base changes were made, one for the cysteine to tryptophan conversion, a silent change to disrupt the PAM (protospacer adjacent motif) and prevent re-cutting of the repaired DNA sequence, and two additional silent changes to generate a diagnostic PstI site. The mutated bases at oligo donor sequence are in boldface. (b) PCR products from genotyping of mice with homozygous allele using the following sequencing primers (F5' – AGGAGGTCCAAATGCTGTT and R5' – GGGAAGGGCGGTAGATG). Sequence across target region confirmed correct introduction of mutations. Red arrows: mutation loci.

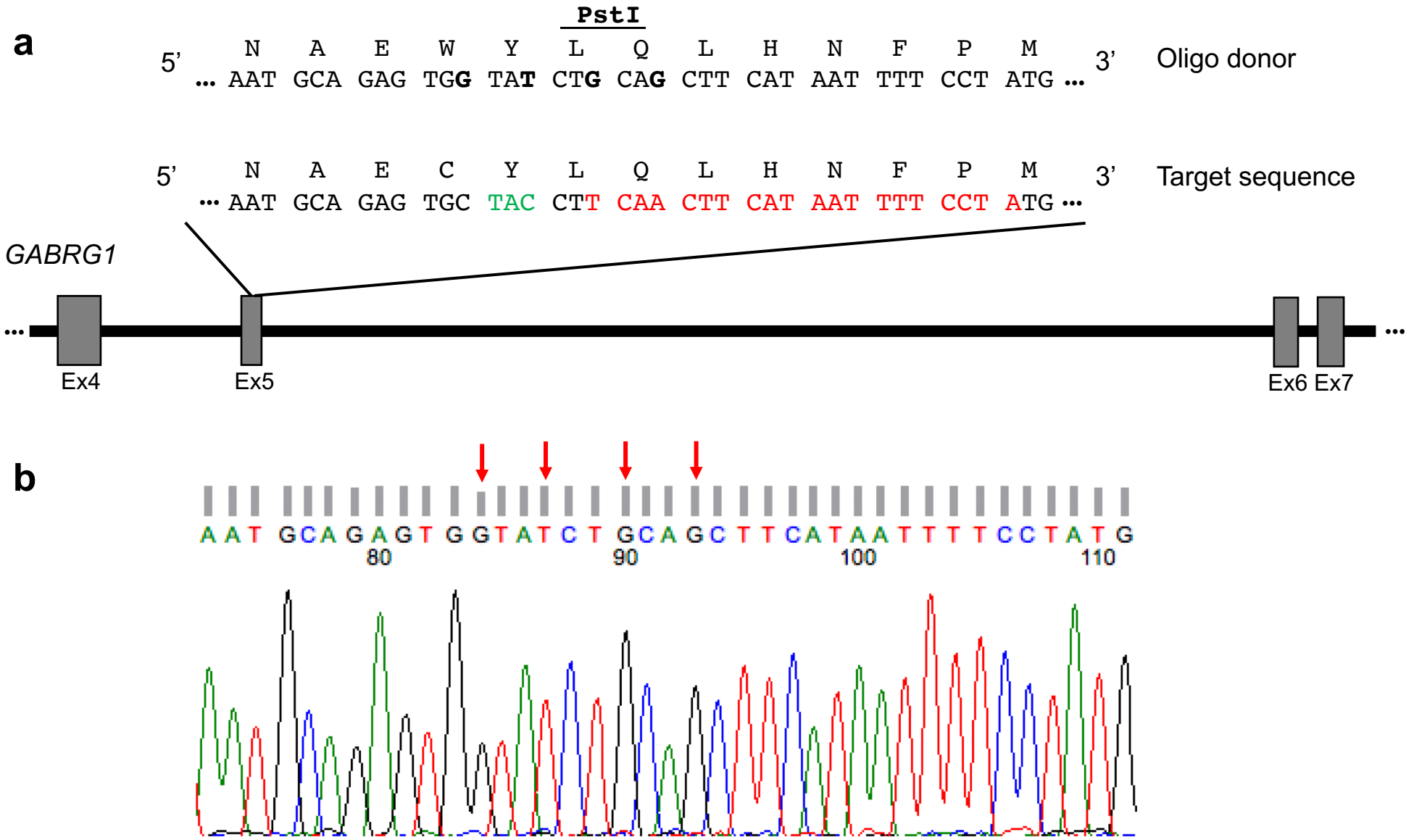

Figure S3. **Structural modelling of *CACNA1H* and *CACNA1F* variants, related to Figure 3.** (a-n) *CACNA1H* variants. S187L (a) wild-type and (b) mutated. The hydroxyl group in Ser187 can form hydrogen bond interactions with the backbone carbonyl oxygen atoms of M183 and M184. Mutation to a hydrophobic L187 disrupts these interactions (ΔΔG = 0.12 kcal/mol). E286K (c) wild-type and (d) mutated. A protonated H355 can form a hydrogen bond with E286. However, the lysyl side chain of K286 is too bulky for that site. Additionally there would be a positive charge repulsion between the side chain resulting in destabilization of the region (ΔΔG = 4.62 kcal/mol). A802V (e) wild-type and (f) mutated. A802 positioned between two helices is surrounded by hydrophobic residues. The larger side chain of V802 can alter nearby helical packing (ΔΔG = 2.06 kcal/mol). E819K (g) wild-type and (h) mutated. Several negatively charged amino acids are clustered around E819. The mutation to a positively charged lysine alters the surface electrostatic charge, potentially destabilizing local secondary structure (ΔΔG = 0.96 kcal/mol). P1605H (i) wild-type and (j) mutated. P1605 positioned at the end of a helix introduces a kink that cannot be replicated by the substituted His residue. R1674H (k) wild-type and (l) mutated. R1674 forms an ion pair with E1865. The ion pair is weakened and may be rendered pH-dependent, likely altering local structure (ΔΔG = 0.53 kcal/mol). R1736C (m) wild-type and (n) mutated. The guanidinium side chain of R1736 forms three hydrogen bonds to the backbone carbonyl oxygens of K1730, L1666 and K1667, and L1668. Loss of these interactions in the R1736 mutant greatly destabilizes the local structure (ΔΔG = 6.79 kcal/mol). The other variants could not be modelled due to absence of template. (o-t) *CACNA1F* variants. I721V (o) wild-type and (p) mutated. I721 lies in a shallow hydrophobic pocket and forms van der Waals interactions with I310, M717 and M732. The strength of the interactions with these residues, especially M717, will be reduced for valine, as its side chain is smaller than that of isoleucine (ΔΔG = 0.78 kcal/mol). R1289G (q) wild-type and (r) mutated. R1289 tethers a helix to a loop by making an ion pair interaction with D1223. Mutation to glycine will disrupt the interactions and change the shape of the loop (ΔΔG = 1.04 kcal/mol). A1335T (s) wild-type and (t) mutated. A1335 lies in the middle in a hydrophobic region in the middle of a helix. Mutation to a polar residue as threonine will change the environment and modestly destabilize the helix (ΔΔG = 0.62 kcal/mol).

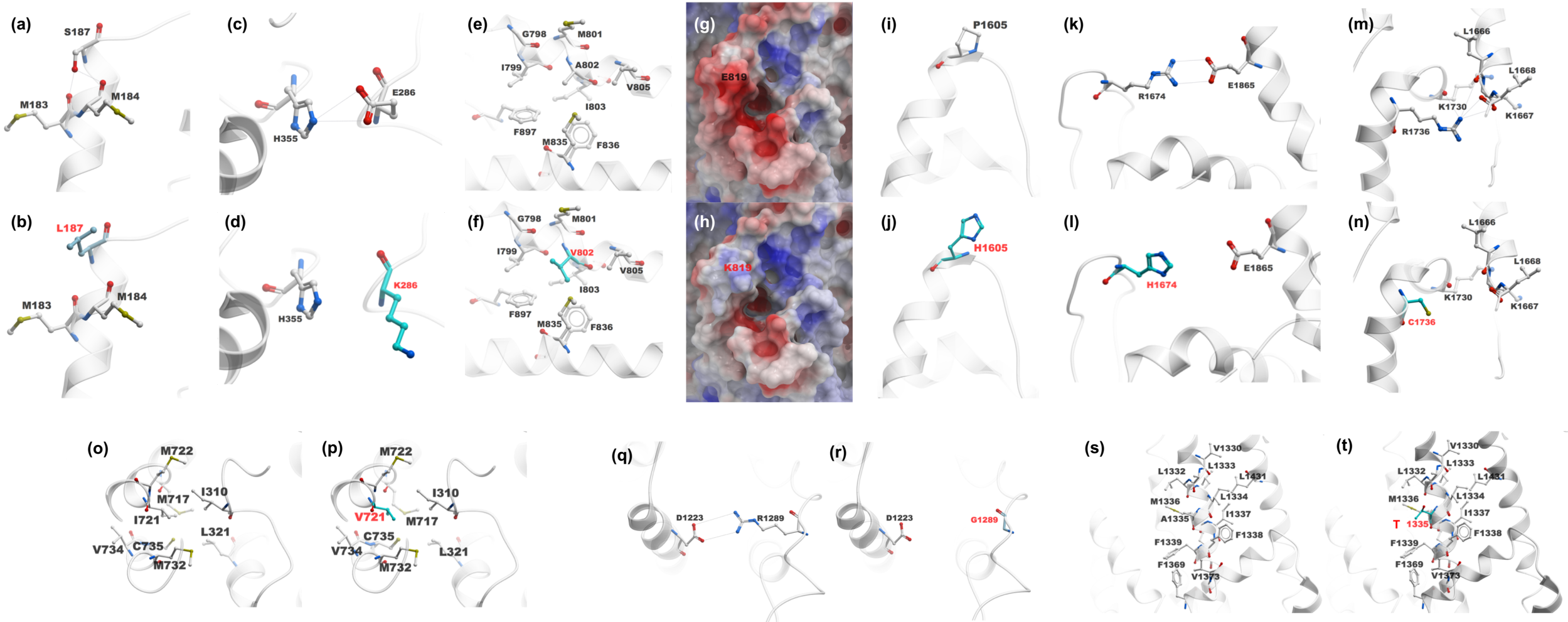

Figure S4. Gnome-wide association analysis (GWAS) and power calculation, related to Table 1. (a-b) GWAS of 236 European cases with TN and 348,028 ethnicity-matched controls from UK Biobank. (a) Manhattan plot for p-values resulting from GWAS. (b) Quantile-quantile plot of observed versus expected p-values. No variants reach genome-wide significance ($P < 5\times10^{-8}$). (c) Power calculation for GWAS of trigeminal neuralgia. Assuming a population prevalence of disease of 0.2%, the graphs show calculated power under lambda = 1.1, 1.2, 1.3, 1.4 at different minor allele frequencies and sample sizes (half of the samples are cases and half are controls).

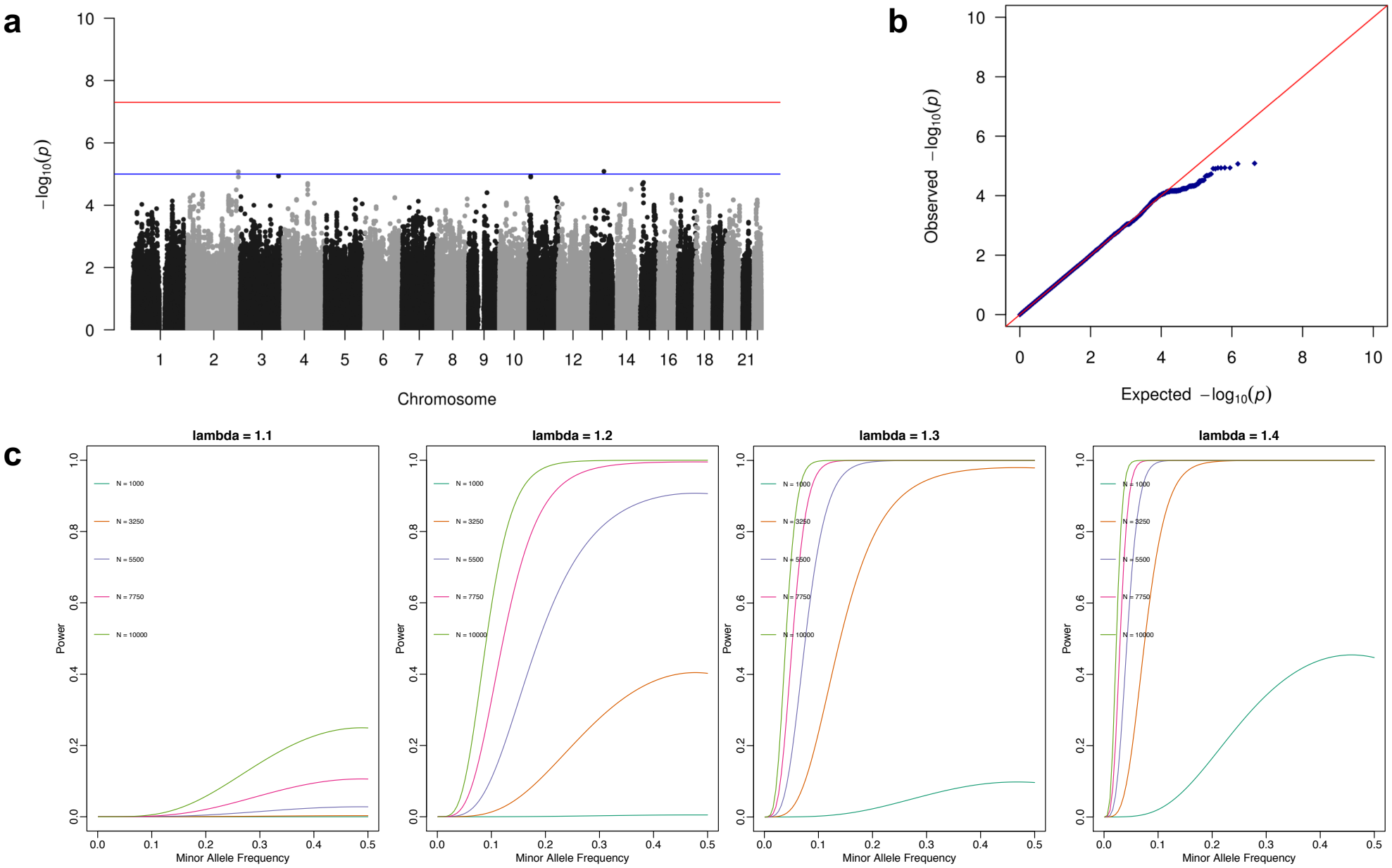

TRANSPARENT METHODS

Case cohort, enrollment, phenotyping, and exclusion criteria

249 probands and their relatives for this study were ascertained from the Yale Facial Pain Clinic; from collaborating institutions; or by responding to a study invitation posted on social media. Written informed consent for genetic studies was obtained from all participants. Parent or legal guardian authorization was obtained in writing for sample collection of all minors in this study. All study protocols were approved by the Yale Human Research Protection Program and Institutional Review Board. Patients and participating family members provided buccal swab samples (Isohelix SK-2S DNA buccal swab kits), medical records, radiological imaging studies and official written reports, and neurosurgery operative reports when available. Inclusion criteria included a diagnosis of either classical trigeminal neuralgia (13.1.1.1) or idiopathic trigeminal neuralgia (13.1.1.3) (Society, 2018) by a neurologist or neurosurgeon. Participants were further subdivided into either "13.1.1.1.1 Classical TN, purely paroxysmal" ("cTN-1") and "13.1.1.1.2 Classical TN with concomitant continuous pain" ("cTN-2"), or "13.1.1.3.1 Idiopathic TN, purely paroxysmal" ("iTN-1") and "13.1.1.3.2 Idiopathic TN with concomitant continuous pain" ("iTN-1"), according to ICHD-3 criteria (Society, 2018) based on phenotypic data. By definition, "13.1.1.2 Secondary TN", including "13.1.1.2.1 TN attributed to multiple sclerosis", "13.1.1.2.2 TN attributed to space-occupying lesion", "13.1.1.2.3 TN attributed to other cause", and "13.1.2 Painful trigeminal neuropathy" related to previous trauma, surgery, or radiation to the trigeminal nerve ipsilateral to pain were excluded from analysis. Also excluded were patients with psychiatric or mental illness that might interfere with patients' ability to grant informed consent or to complete clinical questionnaires.

41 probands with available WES were acquired from UK Biobank with either trigeminal neuralgia (ICD10 code: G50.0) or atypical facial pain (ICD10 code: G50.1) as main diagnosis.

Control cohorts

Controls consisted of 1,798 previously analyzed families with one offspring with autism, one unaffected sibling, and unaffected parents. In this study only the unaffected sibling and parents were analyzed. Controls were designated as unaffected by SSC (Krumm et al., 2015). Permission to access SCC genomic data in the National Institute of Mental Health Data Repository was obtained. Written informed consent for all participants was provided by the Simons Foundation Autism Research Initiative.

Exome sequencing

249 probands and their relatives were sequenced at the Yale Center for Genome Analysis following the same protocol. Briefly, genomic DNA from venous blood or saliva was captured using the Nimblegen SeqxCap EZ MedExome Target Enrichment Kit (Roche) or the xGEN Exome Research Panel v1.0 (IDT) followed by Illumina DNA sequencing (Furey et al., 2018). All Yale and UK Biobank samples were analyzed with the same pipeline. At each site sequence reads were independently mapped to the reference genome (GRCh37) with BWA-MEM and further processed using GATK Best Practices workflows (Genomes Project et al., 2015; McKenna et al., 2010; Van

der Auwera et al., 2013) including duplication marking, indel realignment, and base quality recalibration. Single nucleotide variants and small indels were called using GATK HaplotypeCaller and Freebayes (Garrison E, 2012) and annotated using ANNOVAR (Wang et al., 2010), dbSNP (v138), 1000 Genomes (August 2015)(Genomes Project et al., 2015), NHLBI Exome Variant Server (EVS; https://evs.gs.washington.edu/EVS/), ExAC (v3) (Lek et al., 2016) and Bravo (Program, 2018). The MetaSVM and the Combined Annotation Dependent Deletion (CADD) algorithms were used to predict deleteriousness of missense variants ("D-mis", defined as MetaSVM-deleterious or CADD ≥30) (Dong et al., 2015; Kircher et al., 2014). Candidate variant calls were validated using Sanger sequencing.

Kinship analysis and removal of duplicated samples

Pedigree information and participant relationships were confirmed using pairwise PLINK identity-by-descent (IBD) calculation (Purcell et al., 2007) and pairwise comparison of high quality ultra-rare SNPs absent from public databases (ExAC and gnomAD)(Lek et al., 2016). Individuals with ≥ 90% IBD or shared ultra-rare SNPs were identified as sample duplicates and removed from analysis.

Principal component analysis

EIGENSTAT software (Price et al., 2006) was used to classify ethnicities through analyzing tag SNPs in cases and HapMap samples with known ethnicities. Principal component analysis was then performed to cluster the studied samples with HapMap samples using R software (version 3.4.1) (Wang et al., 2014), and the ethnicities of the cases were determined based on their best clustered ethnicity group against HapMap populations.

Variant filtering

DNMs were called using TrioDenovo (Wei et al., 2015) and filtered using stringent hard cutoffs including: (1) in-cohort allele frequency $\leq 4 \times 10^{-4}$ for controls and MAF $\leq 4 \times 10^{-4}$ across all samples in 1000 Genomes, EVS, and ExAC, Bravo for cases due to limited cohort size, (2) a minimum of 10 total reads total, 5 alternative allele reads, and a minimum of 20% alternate allele ratio in the proband for alternate allele reads ≥ 10 or for alternate allele reads < 10, a minimum 28% alternate ratio, (3) a minimum depth of 10 reference reads and alternate allele ratio < 3.5% in parents, and (4) exonic or canonical splice-site variants.

For transmitted heterozygous variants, we filtered for high-quality heterozygotes (pass GATK Variant Score Quality Recalibration [VQSR], minimum 8 total reads, and genotype quality [GQ] score ≥ 20)(Genomes Project et al., 2015; Lek et al., 2016). Variants with large impact on protein structures including LoF (canonical splice-site, frameshift insertion/deletion, stop-gain, stop-loss) and D-mis variants were considered for the analysis. Common variants with MAF > 5×10^{-3} within the cohort were excluded. Rare variants with MAF ≤ 1×10^{-3} in Bravo were screened in known TN genes. Both ultra-rare (MAF ≤ 1×10^{-5} in Bravo) and moderately rare (MAF ≤ 1×10^{-4} in Bravo) variants were tested for enrichment across all genes of the genome.

We filtered recessive variants for rare (MAF $\leq 10^{-3}$ in Bravo and in-cohort MAF $\leq 5\times10^{-3}$) homozygous and compound heterozygous variants that exhibited high quality sequence reads (pass GATK VSQR, have ≥ 4 total reads for homozygous and ≥ 8 reads for compound heterozygous variants, have a GQ ≥ 10 for homozygous and GQ ≥ 20 for compound heterozygous variants). Only LoF, D-mis, and non-frameshift indels were considered potentially damaging to the disease.

Hemizygous variants were filtered by the same criteria as were recessive variants except for a more stringent frequency filter (MAF $\leq 5\times10^{-5}$ in Bravo and in-cohort MAF $\leq 5\times10^{-3}$).

Segregated variants in familial cases were filtered for rare (MAF $\leq 5\times10^{-4}$ in Bravo and in-cohort MAF $\leq 5\times10^{-3}$) and damaging (LoF and D-mis) dominant variants shared by affected individuals.

Finally, *in silico* visualization was performed on all *de novo*, heterozygous, recessive variants, and hemizygous variants that (1) appeared at least twice, (2) were among the top 20 significant genes from the burden analysis, or (3) segregated in the families. Sanger validation was performed on candidate variants of interest.

De novo enrichment analysis

The expected number of DNM per gene per variant class was obtained based on a mutation model developed previously (Samocha et al., 2014). A one-tail Poisson test was used to compare the observed number of DNMs across each variant class to the expected number under the null hypothesis. The R package 'denovolyzeR' (Ware et al., 2015) was used to perform all *de novo* analyses.

Gene Ontology Enrichment Analysis

Functional profiling of 10 genes with high brain expression (brain expression rank $\geq 75\%$) (Flegel et al., 2015) harboring DNMs was conducted with g:GOSt from g:Profiler (Raudvere et al., 2019), a tool that performs gene set overrepresentation/enrichment analysis and detects statistically enriched terms from functional information sources, including the Gene Ontology database (Ashburner et al., 2000; The Gene Ontology, 2019). We used all annotated genes as the statistical domain scope, the g:SCS algorithm (Raudvere et al., 2019) to address multiple testing, and $p = 0.05$ as a user-defined threshold for statistical significance.

Case-control burden analysis

Case and control cohorts were processed using the same pipeline and filtered with the same criteria (see **Variant filtering** section). A one-sided Fisher's exact test was used to compare the observed number of mutations in each variant class examined in cases to the same variant class in controls under the null hypothesis. The gnomAD controls we used are without TOPMed samples.

Copy number variation analysis

To identify CNVs from WES data, the aligned reads were imported into XHMM (eXome-Hidden Markov Model) (Fromer et al., 2012). Potential CNVs were inspected visually and prioritized

based on Phred-scaled quality score (SQ ≥ 90), genomic length, GC content of targets, and low sequence complexity. CNVs were further annotated by their MAF in gnomAD and 1000 genome databases. Only rare CNVs with MAF ≤ 1×10^{-3} in the above two databases were kept.

Protein structural modelling

The sequence of human SCN5A protein was downloaded from UniProt (Q14524) and aligned with the cryo-electron microscopy structure of the human Nav1.2-beta2-KIIIA (PDB: 6J8E, resolution: 3.00 Å) in ICM-Molsoft (Abagyan et al., 1994; Pan et al., 2019). The homology model was built in ICM-Molsoft based on an 80% sequence identity over resolved residues of human Nav1.2-beta2-KIIIA complex.

The sequence of human CACNA1H protein was downloaded from UniProt (O95180). The structures of the human Cav3.1 (PDB: 6KZO, resolution 3.3 Å) and rabbit Cav1.1 complex (PDB: 5GJW, resolution: 3.6 Å) were used to model the protein using homology tool of ICM-Pro (Wu et al., 2016; Zhao et al., 2019).The initial model was built based on an 85% sequence identity over the resolved residues of human Cav3.1. As the homologous sequence for the loop harbouring residue of interest (R1674) and the surrounding region between 1562-1619 residues were missing in the structure of human Cav3.1, it was built using rabbit Cav1.1 as the template.

The sequence of human CACNA1F protein was downloaded from UniProt (O60840) and aligned with the cryo-electron microscopy structure of the rabbit Cav1.1 complex (PDB: 5GJV, resolution: 3.6 Å) in MolSoft ICM-Pro ver 1.8.7c (Abagyan et al., 1994; Wu et al., 2016). The homology model was built in ICM-Pro based on a 75% sequence identity over the resolved residues of rabbit Cav1.1 complex. All the investigated residues lie in the conserved region of the protein.

The sequence for human GABRG1 protein was obtained from UNIPROT as accession number Q8N1C3. The downloaded Protein Data Bank structure (PDB: 6D6U) was used as a template to construct homology models using MODELLER (Fiser and Sali, 2003).

Twenty models were subjected to restrained energy minimization to relieve steric clashes between or among side chains. Stereochemical parameters were analyzed using PROCHECK (Laskowski et al., 1993) and PROSA (Wiederstein and Sippl, 2007). The final model was chosen based on a combination of the lowest energy function score (Dope) within the modeling program and model satisfaction of standard PROCHECK and PROSA criteria. Mutations were constructed and change of *in silico* free energy (ΔΔG) was calculated using the ICM mutagenesis program (www.molsoft.com) (Abagyan et al., 1994):

$$\Delta\Delta G = \Delta G_{misfolded} - \Delta G_{unfolded}$$

$\Delta G_{unfolded}$ refers to the sum of the energies attributed to the individual residues before the mutation, while $\Delta G_{misfolded}$ refers to the sum of the energies attributed to the individual residues after the mutation. A positive ΔΔG is proportional to the magnitude of the predicted destabilization effect on the protein caused by the point mutation.

Enrichment analysis for the dominant variants

A one-sided binomial test was performed to compare the observed number of damaging dominant variants within each gene with the expected number by the formula below (Jin et al., 2017), and calculated using the following formula:

$$Expected\ Counts_i = N \times \frac{Mutability}{\sum_{Genes} Mutability}$$

where 'i' denotes the 'ith' gene; 'N' denotes the total number of damaging dominant variants; Mutability refers to the *de novo* probability in each gene. The p-value threshold after Bonferroni multiple testing correction is 2.6×10^{-6} (0.05/19,347).

Gabrg1 mouse model and pain testing

The *Gabrg1* knock-in mouse model was generated using CRISPR/Cas9 (Henao-Mejia et al., 2016; Yang et al., 2013). In brief, a T7-sgRNA template was prepared by PCR (Henao-Mejia et al., 2016), incorporating the antisense guide sequence TAGGAAAATTATGAAGTTGA (from the mouse *Gabrg1* gene target region) and then used for *in vitro* transcription and purification with the MEGAshortscript T7 Transcription Kit and MEGAclear Transcription Clean-Up Kit, respectively (both from Thermo Fisher Scientific). Cas9 mRNA (CleanCap, 5moU-modified) was purchased from TriLink Biotechnologies and the homology-directed repair (HDR) oligonucleotide (142 b including 65 b homology flanks was ordered from Integrated DNA Technologies as a phosphorothioate-protected Ultramer. All animal procedures were performed according to NIH guidelines and approved by the Yale IACUC. C57BL6/N strain mice were obtained from Charles River and cytoplasmic microinjections of the sgRNA, Cas9 mRNA and HDR oligo into single-cell embryos were performed by the Yale Genome Editing Center. DNA lysates of tissue biopsies from potential founder pups were screened by PCR amplification with the following primers (F5´-AGGAGGTCCAAATGCTGTT and R5´- GGGAAGGGCGGTAGATG), followed by diagnostic PstI digestion and sequencing confirmation.

Pain hypersensitivity was measured using complementary approaches. Nociceptive withdrawal thresholds of the hind paw and trigeminal nerve region were quantified using the Simplified Up-Down method (SUDO) (Bonin et al., 2014; Taylor et al., 2012). The experimental group consisted of male and female mice carrying homozygous C188W mutations in *Gabrg1*. Sex-matched WT mice were included in the control group. Mice were placed in a transparent Plexiglas cage atop a wire mesh and were free to move about. After 60 minutes of acclimation, withdrawal responses were assessed. To assess sensitivity in the trigeminal nerve regions, Von Frey filaments (Stoelting, USA) were applied perpendicularly to the region of interest. A positive reaction was noted if the animal exhibited a vigorous head retraction or rapid grooming of the muzzle region. The entire SUDO procedure was repeated twice per animal for each nerve region at 5 months of age. A Mann-Whitney test was performed to assess statistical significance of differences between groups. To assess, nocifensive behavior to stimulation of the trigeminal area we also used a complementary modified version of a facial stimulation test (Bailey and Ribeiro-da-Silva, 2006). Mice were stimulated once using filament #7 (0.6 g) and the subsequent grooming response was video recorded. Positive (presence of a stimulus-associated grooming response) and negative responses (absence of grooming behavior) were scored as values of +1 or -1 value, respectively. Mice were

tested 3 times, on different days. Analysis of the videos was assessed by an experimenter blind to the animal's genotype.

Genome-wide association analysis

Imputed genotype array data of 48,7395 samples were obtained from UK Biobank. Only SNPs which have a MAF > 0.05, have a missing genotype rate < 0.01 and passed the Hardy-Weinberg test (H-W p-value > 0.001) were considered for the analysis using plink (Chang et al., 2015). Subjects with self-report and genetically confirmed European ancestry were included (UK Biobank data filed 22006), whereas related subjects (relatedness > 0.1 by gcta64 (Yang et al., 2011)) were excluded. These filters yielded in 236 cases with TN (ICD10 code: G50.0 or G50.1) and 348,028 controls. A Multivariate Logistic Regression was performed using plink (Chang et al., 2015). The covariates included gender and the top 10 principle components. The Manhattan plot was generated using the R (3.4.1) package qqman.

SUPPLEMENTARY REFERENCES

Abagyan, R., Totrov, M., and Kuznetsov, D. (1994). ICM—A new method for protein modeling and design: Applications to docking and structure prediction from the distorted native conformation. Journal of Computational Chemistry *15*, 488-506.

Ashburner, M., Ball, C.A., Blake, J.A., Botstein, D., Butler, H., Cherry, J.M., Davis, A.P., Dolinski, K., Dwight, S.S., Eppig, J.T.*, et al.* (2000). Gene ontology: tool for the unification of biology. The Gene Ontology Consortium. Nat Genet *25*, 25-29.

Bailey, A.L., and Ribeiro-da-Silva, A. (2006). Transient loss of terminals from non-peptidergic nociceptive fibers in the substantia gelatinosa of spinal cord following chronic constriction injury of the sciatic nerve. Neuroscience *138*, 675-690.

Bonin, R.P., Bories, C., and De Koninck, Y. (2014). A simplified up-down method (SUDO) for measuring mechanical nociception in rodents using von Frey filaments. Mol Pain *10*, 26.

Chang, C.C., Chow, C.C., Tellier, L.C., Vattikuti, S., Purcell, S.M., and Lee, J.J. (2015). Second-generation PLINK: rising to the challenge of larger and richer datasets. Gigascience *4*, 7.

Dong, C., Wei, P., Jian, X., Gibbs, R., Boerwinkle, E., Wang, K., and Liu, X. (2015). Comparison and integration of deleteriousness prediction methods for nonsynonymous SNVs in whole exome sequencing studies. Human molecular genetics *24*, 2125-2137.

Fiser, A., and Sali, A. (2003). Modeller: generation and refinement of homology-based protein structure models. Methods Enzymol *374*, 461-491.

Flegel, C., Schobel, N., Altmuller, J., Becker, C., Tannapfel, A., Hatt, H., and Gisselmann, G. (2015). RNA-Seq Analysis of Human Trigeminal and Dorsal Root Ganglia with a Focus on Chemoreceptors. PLoS One *10*, e0128951.

Fromer, M., Moran, J.L., Chambert, K., Banks, E., Bergen, S.E., Ruderfer, D.M., Handsaker, R.E., McCarroll, S.A., O'Donovan, M.C., Owen, M.J.*, et al.* (2012). Discovery and statistical genotyping of copy-number variation from whole-exome sequencing depth. American journal of human genetics *91*, 597-607.

Furey, C.G., Choi, J., Jin, S.C., Zeng, X., Timberlake, A.T., Nelson-Williams, C., Mansuri, M.S., Lu, Q., Duran, D., Panchagnula, S.*, et al.* (2018). De Novo Mutation in Genes Regulating Neural Stem Cell Fate in Human Congenital Hydrocephalus. Neuron *99*, 302-314 e304.

Garrison E, M.G. (2012). Haplotype-based variant detection from short-read sequencing. arXiv *preprint arXiv*, [q-bio.GN].

Genomes Project, C., Auton, A., Brooks, L.D., Durbin, R.M., Garrison, E.P., Kang, H.M., Korbel, J.O., Marchini, J.L., McCarthy, S., McVean, G.A.*, et al.* (2015). A global reference for human genetic variation. Nature *526*, 68-74.

Henao-Mejia, J., Williams, A., Rongvaux, A., Stein, J., Hughes, C., and Flavell, R.A. (2016). Generation of Genetically Modified Mice Using the CRISPR-Cas9 Genome-Editing System. Cold Spring Harb Protoc *2016*, pdb.prot090704.

Jin, S.C., Homsy, J., Zaidi, S., Lu, Q., Morton, S., DePalma, S.R., Zeng, X., Qi, H., Chang, W., Sierant, M.C.*, et al.* (2017). Contribution of rare inherited and de novo variants in 2,871 congenital heart disease probands. Nat Genet *49*, 1593-1601.

Kircher, M., Witten, D.M., Jain, P., O'Roak, B.J., Cooper, G.M., and Shendure, J. (2014). A general framework for estimating the relative pathogenicity of human genetic variants. Nat Genet *46*, 310-315.

Krumm, N., Turner, T.N., Baker, C., Vives, L., Mohajeri, K., Witherspoon, K., Raja, A., Coe, B.P., Stessman, H.A., He, Z.X.*, et al.* (2015). Excess of rare, inherited truncating mutations in autism. Nat Genet *47*, 582-588.

Laskowski, R.A., MacArthur, M.W., Moss, D.S., and Thornton, J.M. (1993). PROCHECK: a program to check the stereochemical quality of protein structures. Journal of Applied Crystallography *26*, 283-291.

Lek, M., Karczewski, K.J., Minikel, E.V., Samocha, K.E., Banks, E., Fennell, T., O'Donnell-Luria, A.H., Ware, J.S., Hill, A.J., Cummings, B.B.*, et al.* (2016). Analysis of protein-coding genetic variation in 60,706 humans. Nature *536*, 285-291.

McKenna, A., Hanna, M., Banks, E., Sivachenko, A., Cibulskis, K., Kernytsky, A., Garimella, K., Altshuler, D., Gabriel, S., Daly, M.*, et al.* (2010). The Genome Analysis Toolkit: a MapReduce framework for analyzing next-generation DNA sequencing data. Genome research *20*, 1297-1303.

Pan, X., Li, Z., Huang, X., Huang, G., Gao, S., Shen, H., Liu, L., Lei, J., and Yan, N. (2019). Molecular basis for pore blockade of human Na⁺ channel Na_v1.2 by the μ-conotoxin KIIIA. Science *363*, 1309-1313.

Price, A.L., Patterson, N.J., Plenge, R.M., Weinblatt, M.E., Shadick, N.A., and Reich, D. (2006). Principal components analysis corrects for stratification in genome-wide association studies. Nat Genet *38*, 904-909.

Program, T.N.T.-O.f.P.M.T.W.G.S. (2018). BRAVO variant browser: University of Michigan and NHLBI. In Available from: https://bravosphumichedu/freeze5/hg38/.

Purcell, S., Neale, B., Todd-Brown, K., Thomas, L., Ferreira, M.A., Bender, D., Maller, J., Sklar, P., de Bakker, P.I., Daly, M.J.*, et al.* (2007). PLINK: a tool set for whole-genome association and population-based linkage analyses. American journal of human genetics *81*, 559-575.

Raudvere, U., Kolberg, L., Kuzmin, I., Arak, T., Adler, P., Peterson, H., and Vilo, J. (2019). g:Profiler: a web server for functional enrichment analysis and conversions of gene lists (2019 update). Nucleic Acids Res *47*, W191-W198.

Samocha, K.E., Robinson, E.B., Sanders, S.J., Stevens, C., Sabo, A., McGrath, L.M., Kosmicki, J.A., Rehnstrom, K., Mallick, S., Kirby, A.*, et al.* (2014). A framework for the interpretation of de novo mutation in human disease. Nat Genet *46*, 944-950.

Society, I.H. (2018). IHS Classification ICHD-3. In 1311 Trigeminal neuralgia (https://www.ichd-3.org/13-painful-cranial-neuropathies-and-other-facial-pains/13-1-trigeminal-neuralgia/13-1-1-classical-trigeminal-neuralgia/: International Headache Society).

Taylor, A.M., Osikowicz, M., and Ribeiro-da-Silva, A. (2012). Consequences of the ablation of nonpeptidergic afferents in an animal model of trigeminal neuropathic pain. Pain *153*, 1311-1319.

The Gene Ontology, C. (2019). The Gene Ontology Resource: 20 years and still GOing strong. Nucleic Acids Res *47*, D330-D338.

Van der Auwera, G.A., Carneiro, M.O., Hartl, C., Poplin, R., Del Angel, G., Levy-Moonshine, A., Jordan, T., Shakir, K., Roazen, D., Thibault, J.*, et al.* (2013). From FastQ data to high confidence variant calls: the Genome Analysis Toolkit best practices pipeline. Curr Protoc Bioinformatics *43*, 11 10 11-33.

Wang, C., Zhan, X., Bragg-Gresham, J., Kang, H.M., Stambolian, D., Chew, E.Y., Branham, K.E., Heckenlively, J., Fulton, R., Wilson, R.K.*, et al.* (2014). Ancestry estimation and control of population stratification for sequence-based association studies. Nature genetics *46*, 409-415.

Wang, K., Li, M., and Hakonarson, H. (2010). ANNOVAR: functional annotation of genetic variants from high-throughput sequencing data. Nucleic Acids Res *38*, e164.

Ware, J.S., Samocha, K.E., Homsy, J., and Daly, M.J. (2015). Interpreting de novo Variation in Human Disease Using denovolyzeR. Curr Protoc Hum Genet, 15.

Wei, Q., Zhan, X., Zhong, X., Liu, Y., Han, Y., Chen, W., and Li, B. (2015). A Bayesian framework for de novo mutation calling in parents-offspring trios. Bioinformatics *31*, 1375-1381.

Wiederstein, M., and Sippl, M.J. (2007). ProSA-web: interactive web service for the recognition of errors in three-dimensional structures of proteins. Nucleic Acids Res *35*, W407-410.

Wu, J., Yan, Z., Li, Z., Qian, X., Lu, S., Dong, M., Zhou, Q., and Yan, N. (2016). Structure of the voltage-gated calcium channel Ca(v)1.1 at 3.6 Å resolution. Nature *537*, 191-196.

Yang, H., Wang, H., Shivalila, C.S., Cheng, A.W., Shi, L., and Jaenisch, R. (2013). One-step generation of mice carrying reporter and conditional alleles by CRISPR/Cas-mediated genome engineering. Cell *154*, 1370-1379.

Yang, J., Lee, S.H., Goddard, M.E., and Visscher, P.M. (2011). GCTA: a tool for genome-wide complex trait analysis. Am J Hum Genet *88*, 76-82.

Zhao, Y., Huang, G., Wu, Q., Wu, K., Li, R., Lei, J., Pan, X., and Yan, N. (2019). Cryo-EM structures of apo and antagonist-bound human Ca(v)3.1. Nature *576*, 492-497.